

Geodetic constraints on contemporary deformation in the northern Walker Lane: 3. Central Nevada seismic belt postseismic relaxation

William C. Hammond*
Corné Kreemer
Geoffrey Blewitt

Nevada Bureau of Mines and Geology, and Nevada Seismological Laboratory, University of Nevada, Reno, Nevada 89557-0178, USA

ABSTRACT

We combine horizontal Global Positioning System (GPS) velocities from a new compilation of published and new GPS velocities, results from an interferometric synthetic aperture radar (InSAR) study, and paleoseismic data to evaluate the postseismic response of historic earthquakes in the Central Nevada seismic belt. We assume that GPS velocity has contributions from time-invariant (i.e., steady permanent crustal deformation) and transient (i.e., time varying and associated with the seismic cycle) processes that are attributable to postseismic viscoelastic relaxation of the crust and upper mantle. In order to infer the viscosity structure of Basin and Range lower crust, η_{LC} , and upper mantle, η_{UM} , we apply three objective criteria to identify rheological models that fit both geodetic and geologic data. The model must (1) improve the apparent mismatch between geodetically and geologically inferred slip rates, (2) explain the InSAR-inferred vertical uplift rate, and (3) not imply time-invariant contractions anywhere in the extending province. It is not required for the postseismic deformation field to resemble the time-invariant velocity field in pattern, rate, or style. We find that the InSAR and horizontal GPS velocities form complementary constraints on the viscoelastic structure, excluding different parts of the model space. The best-fitting model has a lower crust that is stronger than the uppermost mantle, with $\eta_{LC} = 10^{20.5}$ Pa·s and $\eta_{UM} = 10^{19}$ Pa·s, a finding consistent with the majority of similar studies in the Basin and Range. The best-fitting viscosity model implies that the majority of Central Nevada seismic belt deformation is attributable to postseismic relaxation, and hence that western Basin and Range time-invariant deformation north of 39°N latitude is more tightly focused into the northern Walker Lane than would be inferred from uncorrected GPS velocities. However, significant deformation remains after correction for postseismic effects, consistent with Central Nevada seismic belt faults slipping at rates intermediate between the Walker Lane belt and the central Basin and Range.

Keywords: Basin and Range, GPS, earthquake, slip rates, seismic cycle.

*Corresponding author e-mail: whammond@unr.edu.

Hammond, W.C., Kreemer, C., and Blewitt, G., 2009, Geodetic constraints on contemporary deformation in the northern Walker Lane: 3. Central Nevada seismic belt postseismic relaxation, in Oldow, J.S., and Cashman, P.H., eds., Late Cenozoic Structure and Evolution of the Great Basin–Sierra Nevada Transition: Geological Society of America Special Paper 447, p. 33–54, doi: 10.1130/2009.2447(03). For permission to copy, contact editing@geosociety.org. ©2009 The Geological Society of America. All rights reserved.

INTRODUCTION

Rates of slip on active continental faults inferred from geodetic techniques sometimes disagree with the rates inferred from geologic studies. This discrepancy lies near the heart of the relationship between geodetic and geologic investigations of continental deformation (e.g., Friedrich et al., 2003). Similarity of space geodetic and geologic measurements of lithospheric plate motions (DeMets and Dixon, 1999; Sella et al., 2002) has led to anticipation that agreement might occur on the smaller scale of individual faults as well. Where these rates agree, geodetic measurement of relative motions across the fault match the rate inferred from coseismic rupture offset and time between major slip events. However, the comparison requires application of a correction of the geodetic data according to the buried dislocation model, composed of a faulted half space locked at the surface but slipping at depth (Savage and Burford, 1973; Freund and Barnett, 1976). In this case, the cumulative offset of many episodic surface ruptures from the largest earthquakes adds up to the slip predicted by far-field motion of crustal blocks. Some faults, such as the relatively linear and simple San Andreas in central California, exhibit a close agreement (e.g., Murray et al., 2001). This suggests that paleoseismic studies and geodesy measure the same physical processes at play in active faulting, albeit over greatly different time scales and different parts of the seismic cycle. Hence, disagreement between paleoseismic and geodetic slip rates suggests that an explanation is required for the deviation from this paradigm, and perhaps a modification of our physical model.

The Central Nevada seismic belt, which resides near the middle of the Basin and Range Province (Wallace, 1984b), is a well-documented example of disagreement between slip rates estimated with geodetic and geologic techniques. The Central Nevada seismic belt is a quasi-linear sequence of large-magnitude historical earthquakes that form an approximately north-south-trending belt (Fig. 1) (Caskey et al., 2000). The belt remains seismically active to this day, and it is responsible for a large proportion of the total historic seismic moment released in the Basin and Range Province (Pancha et al., 2006). Paleoseismically inferred slip rates for the set of faults that make up the belt near latitude 39°N total probably less than 1 mm/yr (Bell et al., 2004). Geodetic rates, however, inferred mostly from surveys with global positioning system (GPS) are closer to 3–4 mm/yr (Thatcher et al., 1999; Bennett et al., 2003; Hammond and Thatcher, 2004), a difference that is well outside the uncertainties in the measurements.

Recognition of the Central Nevada seismic belt as a zone of recent earthquakes is essential to explaining the discrepancy between geodetic and geologic rates because it allows for the possibility of geodetic strain rates being influenced by transient postseismic relaxation. A number of studies have identified a postseismic response to large earthquakes that has been explained by the viscoelastic properties of Earth's lower crust and upper mantle (starting with Nur and Mavko [1974] and Savage and Prescott [1978]). The transient postseismic part of the earthquake cycle may not be detectable in some cases because the response

decreases to zero over time, and the time since the last earthquake may have been long. Recent progress in modeling the time-dependent surface deformation response (Pollitz, 1997) has made practicable the quantitative constraint of the viscous component of the rheology based on geodetic data.

In what follows, we present a new approach for constraining the viscoelastic properties of the lower crust and upper mantle. We apply three types of complementary data: horizontal GPS velocities, interferometric synthetic aperture radar (InSAR), which is predominantly sensitive to vertical motion, and paleoseismic estimates of fault slip rates and style. When comparing deformation measured with geodesy (e.g., GPS and InSAR) to deformation inferred from geology, we must account for the very different time scales measured with these techniques. In this study, we define time-invariant motion as the hypothetical steady tectonic deformation that occurs at a constant rate over many seismic cycles (e.g., associated with steady motion of the Sierra Nevada with respect to the Great Basin). We define transient motions as those that vary over time scales on the order of the seismic cycle (e.g., exponentially decaying postseismic relaxation of viscous material). Because motions that are measured with GPS at any given time are influenced by time-invariant and transient contributions, we cannot separate these processes if we assume that the predicted relaxation signal resembles the GPS velocity field. Instead, we here assume that the paleoseismic data constrain the time-invariant component of deformation, while physical models of viscoelastic relaxation constrain the complementary transient motion.

In our modeling, we calculate the postseismic velocities expected from the historic earthquakes in the Central Nevada seismic belt and many assumed viscoelastic Earth models, where we vary the viscosity of the lower crust and upper mantle. From each model, we infer the associated time-invariant deformation patterns by subtracting the transient component from the GPS velocities. To evaluate each model, we use misfit criteria based on three types of data: GPS velocities, interferometric synthetic aperture radar results (InSAR), and geologic estimates of fault slip rates. The best models must (1) explain the discrepancy between geologic and geodetic slip rate at the Central Nevada seismic belt, (2) explain the vertical motion observed with InSAR, and (3) not predict time-invariant contractions anywhere in the extensional Basin and Range Province. From the best-fitting viscoelastic Earth model, we obtain the most likely postseismic relaxation two-dimensional surface velocity pattern present inside the current snapshot of the geodetic velocity field. We then present the deformation patterns implied by the estimated time-invariant velocity field and the ways in which they differ from the apparent motion gleaned directly from GPS and other geodetic studies.

DATA

Historic Earthquakes of the Central Nevada Seismic Belt

We consider seismic events in central Nevada occurring in the past 150 yr that had magnitude of ~ 6.5 or above (Table 1).

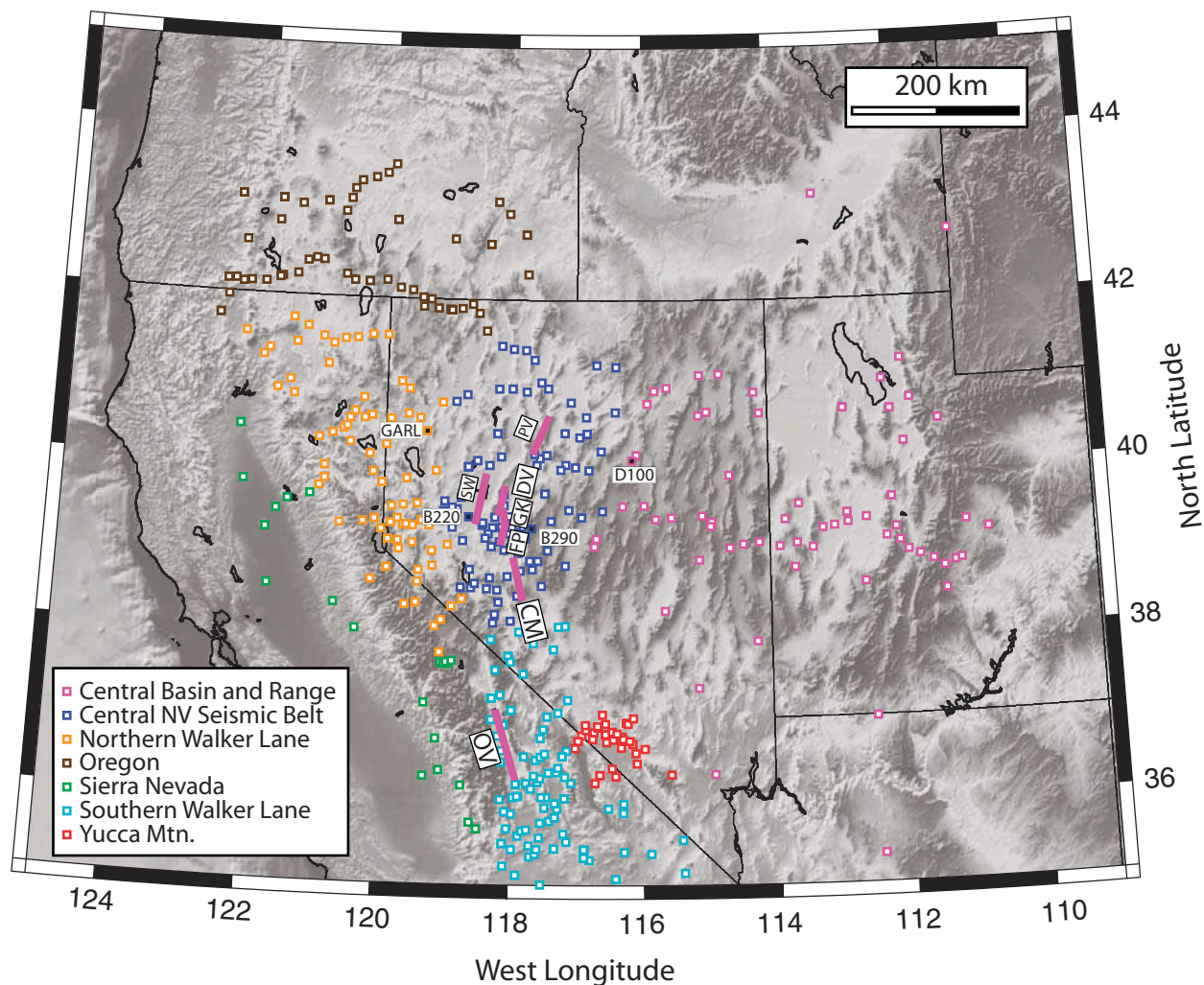


Figure 1. Horizontal velocities for global positioning system (GPS) sites used to constrain the viscosity of the Basin and Range lower crust and upper mantle. Site color designates the strain rate subnetwork discussed in text. Magenta line segments are the fault segments used to model the postseismic relaxation from the Central Nevada seismic belt historic earthquakes. See text for details of fault segments and coseismic slip parameters. Sites labeled GEARL, B220, B290, and D100 and having black interiors are discussed in the text. Fault segments are: CM—Cedar Mountain; DV—Dixie Valley; GK—Gold King–Louderback sequence; FP—Fairview Peak; OV—Owens Valley; PV—Pleasant Valley; SW—Stillwater sequence.

TABLE 1. PARAMETERS USED FOR THE CENTRAL NEVADA SEISMIC BELT EARTHQUAKES

| Earthquake | Date | Fault plane | | | | Slip offset | | Mo (N-m) | M_w |
|---|--|----------------|---------------|------------|---------------|---------------|-------------|----------------------|-------|
| | | Length (km) | Width (km) | Dip (°) | Strike (°) | Displ. (m) | Rake (°) | | |
| Owens Valley | 26 March 1872 | 100 | 15.0 | 90 | 339 | 6.0 | 180 | 2.7×10^{20} | 7.6 |
| Pleasant Valley | 3 October 1915 | 59 | 21.2 | 45 W | 210 | 4.0 | -90 | 1.5×10^{20} | 7.4 |
| Cedar Mountain | 21 December 1932 | 60 | 15.2 | 80 E | 344 | 2.0 | 180 | 5.5×10^{19} | 7.1 |
| Combination of Rainbow Mtn. Fourmile Flat Stillwater | 6 July 1954 6 July 1954 23 August 1954 | 70 | 19.6 | 50 E | 15 | 1.0 | -159 | 4.1×10^{19} | 7.0 |
| Fairview Peak | 16 December 1954 | 32 | 17.3 | 60 E | 15 | 2.4 | -126 | 4.0×10^{19} | 7.0 |
| Combination of Gold King Louderback West Gate | 16 December 1954 16 December 1954 16 December 1954 | 22 | 17.3 | 60 W | 170 | 0.6 | -146 | 6.9×10^{18} | 6.5 |
| Dixie Valley | 16 December 1954 | 42 | 23.3 | 40 E | 17 | 0.9 | -90 | 2.6×10^{19} | 6.9 |

The amount of postseismic motion that a GPS site might detect is a function of the size of the earthquake, its style and orientation, and the time and distance between the event and observation (Pollitz, 1997). For the earthquakes used here (simplified surface traces shown in Fig. 1), these parameters are constrained by geologic and paleoseismic investigation of the earthquake surface ruptures, seismic data, and eyewitness accounts of the earthquakes. Details of the earthquakes are discussed later, and the parameters used in the modeling are in listed Table 1. Our estimates of the moment magnitude, M_w , are, in all cases, within 0.2 of the estimates made by Pancha et al. (2006) for the largest earthquakes in the Basin and Range Province.

Earthquake Characteristics

Owens Valley (1872) M_w 7.6

This event was likely the largest to occur in the Basin and Range Province in historic time (Pancha et al., 2006), and it is the earliest and southernmost event considered. Its mechanism was predominantly right-lateral strike slip with a minor amount of normal, down-to-the-east slip (Beanland and Clark, 1994). The estimated times of previous events on this fault imply that its Holocene slip rate (2–4 mm/yr) (Lee et al., 2001) is among the fastest in the province. Geodetic rates (5–7 mm/yr) are even faster, however, and postseismic relaxation following the 1872 event has been invoked as a possible explanation for this apparent discrepancy (Miller et al., 2001a; Dixon et al., 2003).

Pleasant Valley (1915) M_w 7.4

Occurring at the northern end of the Central Nevada seismic belt, this event was recorded with early-generation seismic instrumentation that was sufficient to characterize its size and tensor moment (Doser, 1988), and it produced 59 km of surface rupture (Wallace, 1984a) that is clearly visible today. Its mechanism was predominantly normal, with extension oriented N65°W.

Cedar Mountain (1932) M_w 7.1

The rupture from this earthquake crossed through three valley fault systems, activating north-south-striking right-lateral strike-slip faults in Monte Cristo Valley, right-lateral and normal faults in Stewart Valley, and secondary north-northeast-striking normal faulting in Gabbs Valley (Bell et al., 1999). The seismic data favor a predominantly strike-slip earthquake on a fault dipping steeply to the east, containing two subevents separated by 10 s (Doser, 1988). In our modeling, the combined static stress changes of both events are what initiate and drive the postseismic response, so we simplify the calculations by assuming a single event that has the surface trace and combined moment of both subevents.

Rainbow Mountain, Fourmile Flat, Stillwater (1954) M_w 7.0

These events occurred in July and August in the same year, prior to the Fairview Peak–Dixie Valley earthquake sequence (Caskey et al., 2004). Their surface traces lie mostly in the eastern part of the Carson Sink, one valley west of the Fairview Peak–

Dixie Valley sequence (Caskey et al., 2004). The Stillwater (M_s 7.0) event was the largest (Doser, 1986), but it was similar to the others in style, consisting of a combination of right-lateral and down-to-the-west normal slip. Because of their similar style and close proximity in time, in our modeling, we combine these events into a single event with the combined moment of all three.

Fairview Peak (1954) M_w 7.0

The coseismic offset parameters for this event are constrained by a combination of paleoseismic (Slemmons, 1957; Caskey et al., 1996) and geodetic data (Savage and Hastie, 1969; Snay et al., 1985; Hodgkinson et al., 1996). Slip was right lateral and normal on an east-dipping fault. This rupture, and the ones discussed later, occupy the middle latitudes of the Central Nevada seismic belt and are hence transitional between the predominantly strike-slip faults to the south (e.g., Owens Valley and Cedar Mountain) and normal ruptures to the north (e.g., Pleasant Valley). The prior event on this fault was likely over 35,000 yr ago (Caskey et al., 2000).

Dixie Valley (1954) M_w 6.9

This event followed the Fairview Peak event by 4 min and ruptured the western range front fault in the valley immediately to the north (Slemmons, 1957). Paleoseismic, geodetic, and seismic data all indicate that it occurred on an east-dipping rupture plane accommodating mostly normal offset (Doser, 1986; Caskey et al., 1996; Hodgkinson et al., 1996). Thus, this event is similar to the Pleasant Valley earthquake, which was the next and northernmost event to the north.

Gold King, Louderback, West Gate (1954) M_w 6.5

These faults likely ruptured simultaneously with the Fairview Peak event. They are west-dipping and lie just north of the Fairview peak rupture. Their distribution is more complex than the other faults, but they are thought to have acted as a geometric link between the ruptures of the Dixie Valley and Fairview Peak earthquakes (Caskey et al., 2000). Individually and combined, they are smaller than the Fairview Peak and Dixie Valley events, so we represent these three ruptures in our modeling as a single event and fault plane consisting of normal and strike-slip offset. Collectively, these three events comprise the smallest event that we consider.

Examination of our final model shows that the smallest earthquakes we consider, the Gold King–Louderback–West Gate sequence (Table 1: M_w 6.5) contributes at most 0.15 mm/yr to the observed GPS velocity field (compared to 2.1 mm/yr for the Owens Valley event). Although some large earthquakes may have occurred in the past (prehistory) that could contribute to transient signals in our GPS data, we have used all the known earthquakes that can significantly affect our results. Given viscosities in the range of 10^{17} – 10^{21} Pa·s (see Table 2 and references therein), a shear modulus of 3×10^{10} Pa, viscous Maxwell relaxation times are on the order of 0.1–1000 yr, and yet Central Nevada seismic belt recurrence intervals are on the order of 5000–35,000 yr (Caskey et al., 2000; Bell et al., 2004; Wesnousky et al., 2005).

TABLE 2. PUBLISHED RESULTS OF LOWER CRUST–UPPERMOST MANTLE VISCOSITIES FOR THE BASIN AND RANGE PROVINCE

| Study | Locality | η_{LC} (Pa·s) | η_{UM} (Pa·s) |
|---|----------------------|--|-------------------------------------|
| <u>Geodetic studies of modern* earthquakes</u> | | | |
| Pollitz (2003) | ECSZ (Mojave) | 3.2×10^{19} | 4.6×10^{18} |
| Pollitz et al. (2001) | ECSZ (Hector Mine) | $\eta_{LC} \gg \eta_{UM}$ | $3\text{--}8 \times 10^{17\dagger}$ |
| Pollitz et al. (2000) | ECSZ (Landers) | $\eta_{LC} \gg \eta_{UM}$ | $1\text{--}6 \times 10^{18}$ |
| <u>Geodetic studies of past earthquakes</u> | | | |
| This study | CNSB/WL/EBR | $1\text{--}3 \times 10^{20}$ | $1\text{--}3 \times 10^{19}$ |
| Gourmelen and Amelung (2005) | CNSB | $>10^{20}$ | $1\text{--}7 \times 10^{18}$ |
| Chang and Smith (2005) | NBR (Hebgen Lk.) | $0.03\text{--}1.3 \times 10^{22}$ | $1.3\text{--}3.2 \times 10^{19}$ |
| Nishimura and Thatcher (2003) | NBR (Hebgen Lk.) | $>10^{20}$ | $10^{18}\text{--}10^{20}$ |
| Hetland and Hager (2003) | CNSB | $5\text{--}50 \times 10^{18}$ | $>10^{19}$ |
| Dixon et al. (2003) | SWL | | 1×10^{19} |
| <u>Geodetic studies of large lake loading/unloading</u> | | | |
| Bills et al. (2007) | WL/CNSB | $2\text{--}10 \times 10^{20}$ | $0.6\text{--}10 \times 10^{18}$ |
| Kaufmann and Amelung (2000) | EBR (Lake Mead) | $>10^{20}$ | $6\text{--}16 \times 10^{18}$ |
| Adams et al. (1999) | WL/CNSB | n.p. | 10^{18} |
| Bills et al. (1994) | EBR (Lk. Bonneville) | $1\text{--}10 \times 10^{20}$ | $\sim 10^{19}$ |
| Nakiboglu and Lambeck (1983) | EBR (Lk. Bonneville) | assumed elastic | $2.1\text{--}34 \times 10^{18}$ |
| <u>Studies of plate-boundary dynamics</u> | | | |
| Flesch et al. (2000) | WL/CNSB | $1\text{--}5 \times 10^{21}$ (whole lithosphere) | |

Note: n.p.—no estimate provided. CNSB—Central Nevada seismic belt, WL—Walker Lane, SWL—southern Walker Lane, ECSZ—Eastern California shear zone, EBR—eastern Basin and Range, NBR—northern Basin and Range.

*Modern earthquakes had coseismic deformation observed with space geodesy.

†Tends to increase toward $1\text{--}3 \times 10^{19}$ after 1–3 yr of relaxation, indicating transient rheology.

Thus, the GPS measurements were made very early in the seismic cycle for Central Nevada seismic belt faults. Because the expected relaxation times are so much shorter than the recurrence intervals, the effects from the penultimate earthquakes are almost certainly negligible and are not modeled.

Global Positioning System Data

We use the horizontal GPS velocities from the compilation of Kreemer et al. (this volume), which includes our own solutions for the continuously recording BARGEN network (Wernicke et al., 2000; Bennett et al., 2003), and also the published and updated velocities from about a dozen campaign networks (see Table 1 of Kreemer et al., this volume, and references therein). The individual velocity solution sets are transformed so that they refer to the Stable North America Reference Frame (SNARF) (Blewitt et al., 2005). The resulting velocity field spans the majority of the Basin and Range Province in California, Nevada, Utah, Arizona, Oregon, and Idaho. The sites are shown in Figure 1, and the velocities are shown in Kreemer et al. (this volume). While the velocity map has spatial density of sites that is highly variable (from less than tens to hundreds of kilometers), the coverage in the vicinity of the Central Nevada seismic belt has at least a dozen sites within 30 km of every fault segment.

Interferometric Synthetic Aperture Radar (InSAR)

We use the InSAR results of Gourmelen and Amelung (2005), which measure the change in range between the surface

and a satellite in low Earth orbit over time. They stacked numerous interferograms constructed from repeat passes of the radar satellite over the Central Nevada seismic belt in order to cancel noise and reduce the uncertainty in the rate of movement. They argued that most of the surface motion observed at the Central Nevada seismic belt using this technique is attributable to vertical motion of the surface because the horizontal GPS signal in the same area (Hammond and Thatcher, 2004) cannot explain the InSAR data. Thus, the observations are most consistent with a domelike uplift with a rate of 2–3 mm/yr centered over the Fairview Peak–Dixie Valley–Pleasant Valley ruptures. This uplift is not well observed in the GPS measurements because the uncertainties in the vertical component of GPS are a factor of three to four larger than in the horizontal and exceed the signal observed by Gourmelen and Amelung (2005). Other GPS sites that are continuously recording, such as the BARGEN network (Bennett et al., 1998; Wernicke et al., 2000), or that have had significantly longer observation history, such as the Basin and Range Highway 50 network (Thatcher et al., 1999; Hammond and Thatcher, 2004), are not ideally positioned to observe the uplift seen with InSAR, since they lie to the south, east, or west of the maximum of the bulge. Thus, the InSAR measurements currently represent the best available source of relative vertical motion across the Central Nevada seismic belt.

The U.S. Geological Survey Quaternary Fault and Fold Database

We use data from the U.S. Geological Survey (USGS) Quaternary Fault and Fold database in the Basin and Range and

California (hereafter referred to as UQFD; Haller et al., 2002; Cao et al., 2003) to constrain the amount of permanent tectonic deformation that has occurred in the Basin and Range in the recent geologic past. A live internet accessible version of this database is available at <http://earthquake.usgs.gov/qfaults/>, but we used the specific tables associated with the Haller et al. (2002) and Cao et al. (2003) publications. It contains a compilation of fault geometries in the United States and associated estimates of slip direction and rate when available. In addition, we include results from the more recent study of paleoseismic slip rates for the Central Nevada seismic belt (Bell et al., 2004) and the compilation of dePolo and Anderson (2000), who used a reconnaissance technique to estimate rates of slip on 45 normal faults in the Basin and Range. Since their technique tends to identify an upper bound to slip rate, and we used these rates whenever available, our inferred rates of geologic moment release may be similarly high. The information contained in these databases is complementary to geodetic data that measure contemporary surface deformation. The geodetic velocity field may include transients that are not representative of time-invariant (i.e., many times greater than a seismic cycle) behavior or permanent deformation. In contrast, paleoseismic data constrain the age, location, and style of permanent surface deformation accommodated by slip on faults. If tectonic deformation progresses at a constant rate over time, then paleoseismology should constrain the same horizontal deformation field on Earth's surface that is measured by geodesy, when adjusted for transient effects.

The fault slip rate information is used to infer horizontal strain rates by using the moment tensor summation method of Shen-Tu et al. (1999), which is based on the approach of Kostrov (1974). We create a map-view grid of the Basin and Range Province with $0.4^\circ \times 0.4^\circ$ horizontal two-dimensional cells. Inside each cell with area A , we calculate the average horizontal strain rate tensor by summing over n fault segments within the cell:

$$\dot{\epsilon}_{ij} = \frac{1}{2} \sum_{k=1}^n \frac{L_k \dot{u}_k}{A \sin \delta_k} m_{ij}^k, \quad (1)$$

where L_k is the length, δ_k is the fault dip angle, and \dot{u}_k is the scalar slip rate of the k th fault. The unit moment tensor m_{ij}^k is defined as $m_{ij}^k = u_i n_j + u_j n_i$, where \mathbf{n} is the horizontal unit vector normal to the fault trace, and \mathbf{u} is the horizontal direction of slip across the fault (Shen-Tu et al., 1999; Kreemer et al., 2000). The horizontal tensor strain rate for each cell is obtained through the summation in Equation 1. The associated vector velocity field can be obtained through integration of the strains plus definition of a reference frame. The resulting map of permanent deformation associated with the fault database is shown in Figure 2.

The resulting strain field obtained from the UQFD (Fig. 2) is similar in spatial pattern and deformation style to that obtained from the geodetic velocity field (method discussed in Kreemer et al., this volume). Both have zones of more rapid deformation in the westernmost 100–200 km of the Basin and Range. Both have zones of right-lateral and extensional slip and have velocities ori-

ented west/northwest that increase and rotate clockwise to the west. The similarity in these two deformation patterns suggests that the geodetic velocity field is dominated by the time-invariant component of deformation. There are, however, a number of differences in the details of the geologic and geodetic models. For example, in general, the geologic strain rates are considerably lower than the geodetic rates. The differences between them may be partly attributable to incompleteness of the catalog of surface faulting (which is spatially variable), and by the presence of transients in the geodetic velocity field caused by postseismic relaxation. Zones of higher rate deformation, associated with an east-west velocity gradient of 2–3 mm/yr, are also located in the vicinity of the Wasatch fault zone at the Great Basin eastern boundary. Note that a small appendage of 4–8 nanostrains/yr strain rate seen in the geologic strain rate map (Fig. 2) near 117°W longitude and 39°N latitude is not located at the Central Nevada seismic belt, but southeast of it. The slightly higher strain rate in this band is controlled by the proximity of several faults with <0.2 mm/yr slip rate estimates (Lone Valley fault, Southwest Reese River Valley, Western Toiyabe Range) and one with 0.22 mm/yr (Toiyabe Range fault zone).

Differences between the geodetic and geologic deformation fields can, at least partially, be explained by the incompleteness of the geologic catalog of prehistoric earthquakes. In a provincewide comparison of seismic, geologic, and geodetic moment rates in the Basin and Range, Pancha et al. (2006) have shown that the rate of geologically inferred moment release is less than that inferred from seismic and geodetic moment rates. They estimated a geodetic moment of between 4 and 7×10^{18} N-m/yr and a geologic moment of 2.5×10^{18} N-m/yr, implying a provincewide value for the ratio of geodetic moment over geologic moment R between 1.6 and 2.8. We calculate our own estimates of the ratio of geodetic over geologic moment rates R for each subdomain shown in Figure 1. To be consistent between our estimates of geodetic and geologic moment, we calculate the average moment for each inside the $0.4^\circ \times 0.4^\circ$ cells that cover each of the regions defined in Figure 1 from the continuum strain rate models. We assume that moment is proportional to the total strain rate defined as the second invariant of the strain rates tensor (Kreemer et al., this volume), and then we sum the moments in each region. The Central Basin and Range (which includes the Wasatch), northern Walker Lane, Yucca Mountain, Oregon, and southern Walker Lane domains have R values of 2.9, 4.9, 2.0, 3.9, and 3.9, respectively. For sites closest to the Central Nevada seismic belt (within ~ 70 km), $R = 9.5$, consistent with the geodetic deformation exhibiting elevated strain rates via transient effects. For a geographically broader selection of sites (within ~ 180 km) centered at the Central Nevada seismic belt, $R = 5.1$, consistent with the presence of enhanced geodetic moment that is focused near the Central Nevada seismic belt.

The relatively high values of R for the northern and southern Walker Lane are driven by geodetic strain rates that are highest at the westernmost boundary of the Basin and Range, adjacent to the Sierra Nevada microplate (Kreemer et al., this volume). In

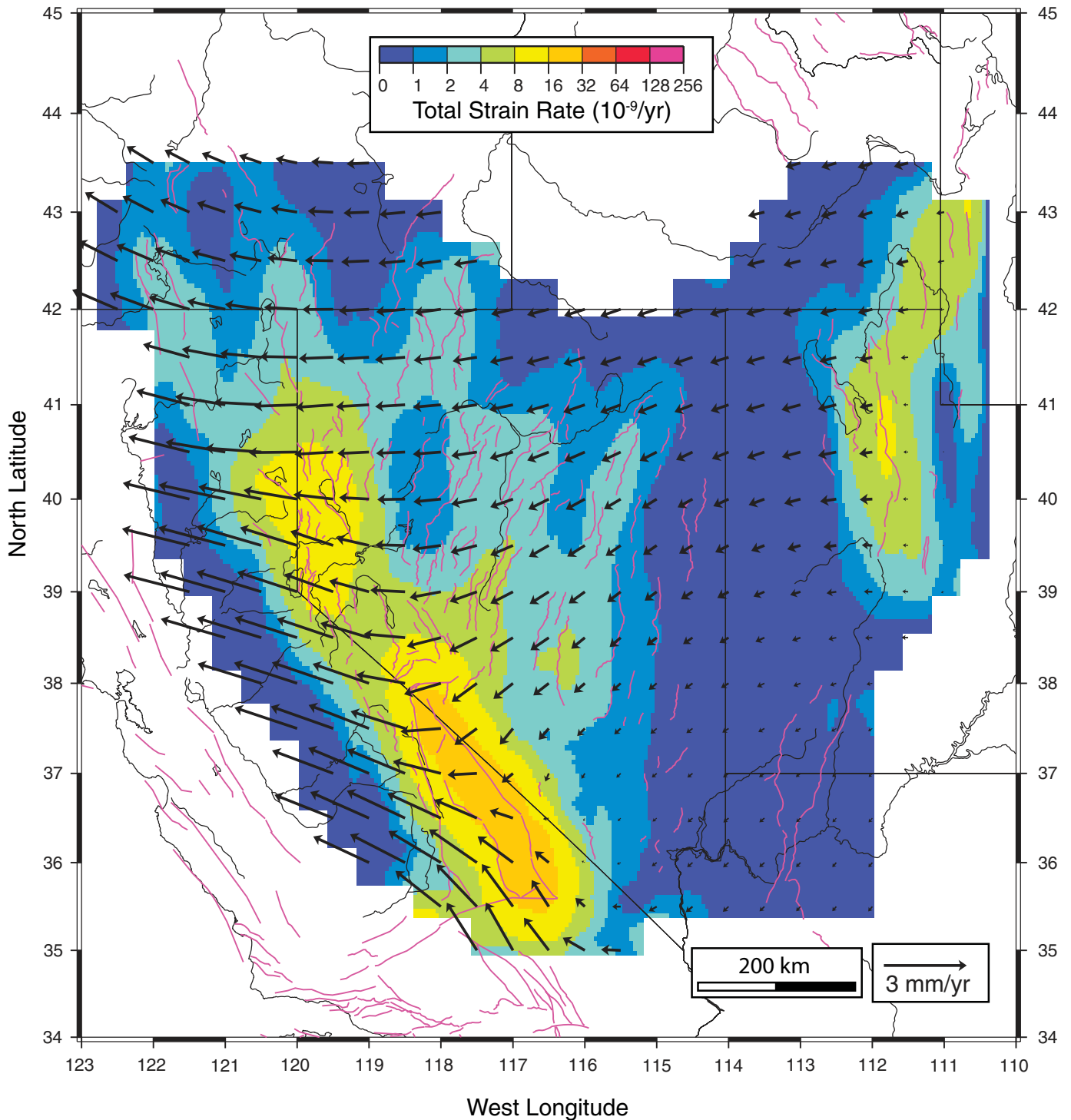


Figure 2. Strain rate field inferred from the paleoseismic databases of the U.S. Geological Survey and dePolo and Anderson (2000). Black arrows are velocities with respect to North America on a regular grid that result from integration of the strain rates. Colors are the second invariant of the strain rate (includes shear and dilatation). Magenta line traces are faults in the database. Note that the finger of higher strain rates near longitude 117°W and latitude 39°N lies east of the Central Nevada seismic belt.

this version of the UQFD, the Mohawk Valley fault is not present and thus effectively has a rate of 0.0 mm/yr. It has been shown recently to have 0.3–0.5 mm/yr slip on a single strand (Sawyer et al., 2005). Also in our version of the UQFD, the Owens Valley fault has a rate of 1.5 mm/yr, which is now estimated in the current version of the database to be 1.0–5.0 mm/yr (<http://earthquake.usgs.gov/qfaults>, accessed March 2007). Thus, it is likely that values for R would be smaller for the southern and northern Walker Lane if they were estimated from a more current UQFD database. The data are also consistent with a province-wide moment rate deficit in the paleoseismic earthquake catalog, of an approximate factor of 3 ± 1 , since areas without significant historic seismic moment release also show a discrepancy.

Another difference between the geologic model (Fig. 2) and the geodetic model (Fig. 3) of Kreemer et al. (this volume) is seen in the azimuth of velocities in southern Nevada, western Utah, and northwest Arizona. In this area, the geologic model velocities have a southwest azimuth, whereas the geodetic model velocities have an azimuth north of west. However, in both models, the tensor strain rates are the primary solution, and velocities are obtained by integrating the strains while defining the velocity reference frame to be zero at the eastern edge of the model, east of the Wasatch fault zone in eastern Utah and southwest Wyoming. Uncertainties in this zero-velocity condition on this boundary allow for a small solid body rotational difference in the velocity fields, with a pole of rotation near the Wasatch. Adjusting for such a rotation could add a northwest component to velocities in southern Nevada, giving them a more western azimuth, without changing the fit to the geologic data. Furthermore, 1–3 mm/yr GPS velocities in southern Nevada and on the Colorado Plateau have a west azimuth and drive the azimuth in the geodetic model. No such constraint exists in the geologic model, since the rates on the Hurricane fault in southwest Utah and northwest Arizona are very low, and strain rates east of the Colorado Plateau are not taken into account. These differences, however, do not affect the strain rate patterns in either figure.

RELAXATION MODELING

There are several lines of evidence that suggest that post-seismic processes are observable decades after the Central Nevada seismic belt earthquakes, and that these are dominated by the process of viscoelastic relaxation of the lower crust and/or upper mantle. These arguments fall into three classes. First, observations of similar-magnitude earthquakes that have occurred during the era of modern geodetic observation have been used to infer upper mantle and lower-crustal viscosities of 10^{17} – 10^{21} Pa·s and rule out other processes, such as poroelastic rebound and afterslip (Pollitz et al., 2000, 2001; Hearn, 2003; Pollitz, 2003). Studies of other mid-twentieth-century Basin and Range earthquakes (e.g., Borah Peak, and Hebgen Lake) (Nishimura and Thatcher, 2003; Chang and Smith, 2008) and Lake Lahontan and Bonneville rebound (Bills and May, 1987; Bills et al., 1994; Adams et al., 1999) have found similar values

for lower crust–upper-mantle viscosities (Table 2). These suggest that the conditions for viscoelastic relaxation are present and will have the decades-long time scale needed to provide a signal in the year 2005. Other processes such as afterslip and poroelastic rebound are not expected to provide observable signals so long after the earthquakes. Second, the Central Nevada seismic belt exhibits a geodetic signature that is consistent with the presence of ongoing viscoelastic relaxation. A broad vertical uplift in the vicinity of the Dixie Valley–Fairview Peak and Pleasant Valley ruptures has been observed using stacks of InSAR scenes (Gourmelen and Amelung, 2005). This horizontal dimension and vertical rate, and decades-long relaxation time scale of this broad bulge, are consistent with viscosities obtained in other studies. Horizontal GPS measurements reveal anomalous dilatation at the Central Nevada seismic belt, which is consistent with this bulge (Hammond and Thatcher, 2004; Kreemer et al., this volume), and contractions east of the Central Nevada seismic belt that are otherwise difficult to reconcile with a region that is undergoing tectonic extension have been tentatively identified (Wernicke et al., 2000; Bennett et al., 2003; Friedrich et al., 2004; Hammond and Thatcher, 2004). Thirdly, the disagreement between geodetic and geologic slip and moment rates is large in the vicinity of the Central Nevada seismic belt ($R = 5.1$ – 9.5) and southern Walker Lane domains ($R = 3.9$), which contain the large historic earthquakes, compared to the adjacent domains. These large R values can be explained by an enhancement of geodetic strain resulting from viscoelastic relaxation. This argument alone is only consistent with relaxation rather than proof of it, however, since regions that have undergone less paleoseismic investigation can have relatively incomplete moment derived from the UQFD.

Modeling: Philosophy and Construction

Considering the previous arguments, we proceed under the assumption that transient deformation in the geodetic signal is caused by viscoelastic postseismic relaxation of the lower crust and upper mantle. However, measurements of the geodetic velocity field at the surface of the planet capture effects related to both time-invariant and transient processes that are a direct manifestation of the earthquake cycle. The transient effects can be related to the observed geodetic velocities via

$$v_{\text{geodesy}} = v_{\text{time-invariant}} + v_{\text{transient}}, \quad (2)$$

where we constrain v_{geodesy} with GPS and InSAR observations, and we constrain $v_{\text{transient}}$ with the physics governing viscoelastic deformation of a layered medium. Equation 2 can also be expressed in terms of the spatial derivatives of velocity, i.e., strain rates, which we use in the criteria for model fit. We consider the time-invariant component of the geodetic velocity field as an unknown and model the transient portion of the velocity field by assuming a layered viscoelastic structure that is stressed by the Central Nevada seismic belt earthquake dislocations given

in Table 1. Thus, for each viscosity structure, there is an associated postseismic transient velocity field and an associated time-invariant velocity field derived from Equation 2.

To model the evolution of the relaxation following the seismic events, we use the spherically layered viscoelastic modeling software VISCO1D (Pollitz, 1997). The software assumes a Newtonian Maxwell viscoelastic rheology and includes the effects of gravitation, which can have minor effects on the relaxation history at long intervals after the earthquake. Because we assume Newtonian rheology, we may sum the independently modeled earthquakes responses in the year 2005 to get the combined response. Although some studies have suggested that power-law, biviscous or transient rheologies are needed to explain the postseismic response, these studies are usually based on data obtained within days to a few years after the earthquake (Pollitz et al., 2001; Pollitz, 2003; Freed and Bürgmann, 2004), when multiple processes may have contributed to the postseismic response (Fialko, 2004). The Maxwell Newtonian rheology is simpler and is usually an adequate explanation of the data on time scales of 10,000–15,000 yr (e.g., Bills et al., 1994; Adams et al., 1999; Hetland and Hager, 2003; Nishimura and Thatcher, 2003; Pollitz et al., 2004). Furthermore, we expect that the mechanisms that have shorter relaxation times (e.g., poroelastic rebound; Fialko, 2004) will have dissipated early in the decades between the time of the GPS measurements and the events we consider. Based on previous structural and dynamic studies, we assume a laterally homogeneous 15-km-thick elastic uppermost layer that represents the upper crust, overlying a 15-km-thick viscoelastic lower crust (Fig. 3). This structure is a simplification based on studies that suggest a flat seismic Moho at 30–35 km depth (e.g., Allmendinger et al., 1987; Benz et al., 1990; Holbrook, 1990; Gilbert and Sheehan, 2004), and a rheological distinction between the lower and upper crust (see references in Table 2). The viscoelastic upper mantle extends from the bottom of the lower crust to a depth of 370 km. We tested models having a deeper bottom to the viscoelastic

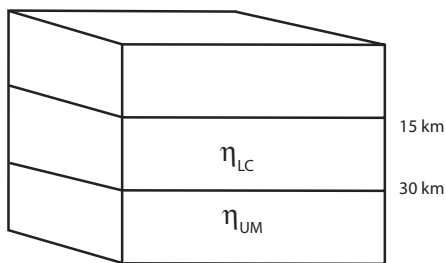


Figure 3. Rheological properties of our model as a function of depth. The uppermost layer (0–15 km) is assumed to be elastic; the lower crust (15–30 km) and upper mantle are assumed to be Maxwell viscoelastic. The elastic modulus μ is obtained from the one-dimensional seismic model PREM (Dziewonski and Anderson, 1981), and viscosities of the lower crust η_{LC} and upper mantle η_{UM} are varied in a grid search.

upper mantle (down to a depth of 1088 km), and these gave nearly identical relaxation velocities (difference less than 0.1 mm/yr). The values for the shear and bulk elastic moduli are from the global one-dimensional seismic model PREM (Dziewonski and Anderson, 1981) mapped into discrete layers of 2–35 km thickness, thickening with depth. The values for the viscosity of the lower-crustal and upper-mantle layers are iteratively selected in a grid search, varying each from 10^{17} to 10^{21} Pa·s in logarithmic steps of one-half order of magnitude. For each model, the velocity in the year 2005 at each of the GPS sites shown in Figure 1 is computed, and these include the combined effects of each of the earthquakes listed in Table 1.

We use the characteristics of both the transient and time-invariant velocity fields to constrain the viscosities of the lower crust and upper mantle. To achieve this, we apply three objective criteria for the elimination of models that violate one or more of our three sources of data: GPS, InSAR, and paleoseismology. We cannot simply compare the results of our calculations to the geodetic observations because only the transient component of the velocity field is obtained in the viscoelastic modeling. Instead, we use the transient model and the observed GPS velocities to estimate the long-term velocity field using Equation 2, and then select a best model based on a synthesis of all of the following three objective, and independent, criteria:

1. The inferred time-invariant velocities in the vicinity of the Central Nevada seismic belt must imply a moment accumulation rate that makes a better match to the geologic moment release rate than do the raw GPS velocities. This criterion is based on the assumption that the mismatch between geodetic and geologic moment rates can be explained, at least in part, by the presence of postseismic viscoelastic relaxation.

2. The transient model must predict the uplift that is observed with InSAR. The vertical contribution from the time-invariant motion is presumed to be negligible at the Central Nevada seismic belt. This is consistent with slip rates, constrained by paleoseismology, that have an extensional component of slip that is less than 0.7 mm/yr total for four faults crossed by U.S. Highway 50 and less than 0.3 mm/yr for each of them (Bell et al., 2004). However, the observed motion is 2–3 mm/yr of surface uplift (Gourmelen and Amelung, 2005), which is at least several times greater than is expected based on strain accumulation. The wavelength of deformation expected from the transient response (>100 km) is much broader and is theoretically separable from the elastic strain response of individual faults (a few tens of kilometers). Thus, the spatial characteristics of the two processes could be used to separate the vertical component of the relaxation signal. However, that work is beyond the scope of this study, and we here assume that the entire vertical signal is attributable to relaxation.

3. The time-invariant model must not predict long-term contraction in regions characterized geologically by tectonic trans-tension. This is identical to, but more generally applied than, the assumption used by Hetland and Hager (2003) in an analysis of the horizontal GPS data of Thatcher et al. (1999) and Wernicke et al. (2000), where they assumed that contraction east of the

Central Nevada seismic belt needed to be explained by the post-seismic model.

These criteria can be more generally applied to tectonically deforming areas that have experienced recent earthquakes that may be affecting the modern geodetic velocity field. Also notice that none of these criteria requires that the postseismic deformation field resemble the time-invariant velocity field in pattern, style, or rate. For the Central Nevada seismic belt, the above criteria select a clearly defined best model, as described next.

Resolving Power of GPS, InSAR, and Geologic Data

The InSAR and horizontal GPS velocities form highly complementary constraints on the upper-mantle and lower-crustal viscoelastic structures. Each data type excludes very different portions of the model space. To evaluate the misfit of the viscosity models to the different types of data, we design the misfit as the combination of three different terms

$$\chi^2 = \alpha(R-1)^2 + \left(\frac{v_u - v_{\text{InSAR}}}{\sigma_{vu}} \right)^2 + \sum_{i=1}^6 \left(\frac{\epsilon_{\Delta}}{\sigma_{\epsilon\Delta}} \right)^2, \quad (3)$$

where R is the ratio of geodetic moment to geologic moment estimated in the Central Nevada seismic belt domain, and v_u is the maximum vertical velocity in the Central Nevada seismic belt domain obtained for each model in the grid search. The quantities v_{InSAR} and σ_{vu} are the vertical rate and its uncertainty observed with InSAR at the Central Nevada seismic belt taken to be 2.5 ± 0.5 mm/yr (Gourmelen and Amelung, 2005). The dilatational strain rate, ϵ_{Δ} , and its uncertainty, $\sigma_{\epsilon\Delta}$, are obtained from the estimated time-invariant velocity field and the formal uncertainty obtained in the strain rate calculation. For the purposes of calculating the misfit, we assign $\epsilon_{\Delta} = 0$ whenever $\epsilon_{\Delta} \geq 0$, so that no extensional deformation, regardless of its rate, will be penalized. The summation in the third term sums the contributions from each of the domains. The Oregon domain is not included because contractions owing to Cascadia interseismic strain accumulation (McCaffrey et al., 2000; Miller et al., 2001b; Svarc et al., 2002a) and from the collision of the Sierra Nevada microplate with the Oregon domain (Hammond and Thatcher, 2005) are likely present and should not be penalized. The resulting misfit surfaces, for each of the terms in Equation 3, and for the combined constraint, are shown in Figure 4. The weight α is applied to control the relative importance of the first term, since it is not normalized by an uncertainty. We begin with a trial value of $\alpha = 1$, and then reduce α until models that are excluded by any single criterion are still excluded by the combined criteria, arriving at $\alpha = 0.7$. In other words, dark regions in Figures 4A–4C are also dark in Figure 4D. This approach gives approximately equal model exclusion power to the first term compared to the second and third terms in Equation 3. The minimum misfit taking all three criteria into account (Fig. 4D) identifies $\eta_{\text{LC}} = 10^{20.5}$ and $\eta_{\text{UM}} = 10^{19}$ as the best-fitting model. This result appears to

agree well with each of the individual criteria, since this model lies inside the region of minimal geologic/geodetic, InSAR, and contraction constraint misfit (Figs. 4A–4C). Models that fit similarly well can be found by decreasing η_{LC} and/or η_{UM} by one-half order of magnitude, but outside the zone defined by the contour where $\chi^2 = 2$, misfits increase rapidly. The misfit in the InSAR term increases most rapidly when η_{UM} is above 10^{19} Pa·s or reduced below $10^{18.5}$ Pa·s. When η_{LC} is decreased, the InSAR constraint yields a greater misfit; however, a more powerful limit on the lower bound of η_{LC} comes from the introduction of time-invariant contractions in the Sierra Nevada and Central Nevada seismic belt domains when η_{LC} is below 10^{20} Pa·s. The lower-crustal viscosity η_{LC} could be greater than $10^{20.5}$ and not strongly violate the InSAR result, but this would come at some cost to the fit between geologic and geodetic data. The precise amount of uncertainty in the estimates of η_{LC} and η_{UM} is difficult to quantify because Equation 3 is not a truly normalized measure of model misfit, and α is subjectively assigned. However, the models outside the $\chi^2 = 4$ combined constraint contour in Figure 4D are being excluded by at least one of the criteria. Thus, uncertainties in η_{LC} and η_{UM} are near one-half order of magnitude.

Results

To guide the evaluation of our results, the sites are divided into separate geographic domains so that different regions can be evaluated individually. These domains are: (1) the southern Walker Lane, (2) the northern Walker Lane, (3) the Sierra Nevada microplate, (4) the Central Nevada seismic belt, (5) southern Oregon, (6) the eastern Basin and Range, and (7) the Yucca Mountain area (Fig. 1). These domains are selected, somewhat subjectively, according to their first-order deformation characteristics based on previous geodetic and geological studies. For each viscoelastic model, we calculate the horizontal tensor strain rate inside each of the subdomains from the estimated time-invariant velocity field. We estimate the three horizontal strain rate parameters ($\epsilon_{\phi\phi}$, $\epsilon_{\lambda\lambda}$, $\epsilon_{\phi\lambda}$) simultaneously with three solid body rotation parameters (latitude [λ], longitude [Φ], and rotation rate [ω]) on the surface of a sphere according to the method of Savage et al. (2001). Figure 5A shows the dilatational component of the strain rate ϵ_{Δ} calculated for sites inside the Central Nevada seismic belt domain and corrected for the effects of postseismic relaxation based on each of the models in our grid search. The strain rate has been normalized by its uncertainty to illustrate the transition to models that imply no significant deformation in the Central Nevada seismic belt domain.

In order to evaluate the models according to our first objective criterion, we examine the ratio of geodetic moment rate corrected for postseismic effects to geologic moment rate in the Central Nevada seismic belt domain. The geologic moment is obtained from the UQFD and Equation 1, while the geodetic moment is obtained from the GPS velocities corrected for postseismic effects via the relaxation models. The modified ratio R is shown as a function of model viscosities in Figure 5B. Because

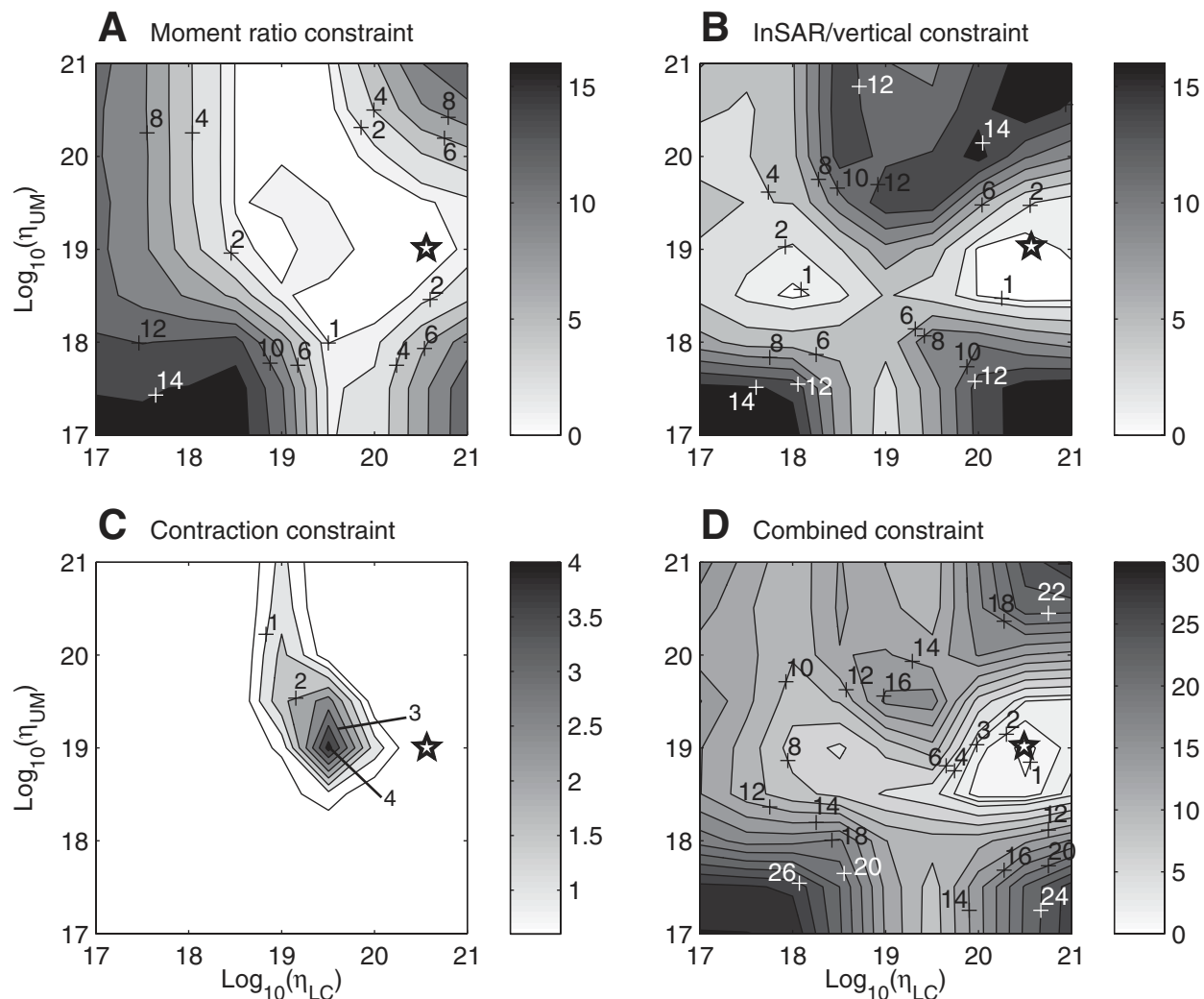


Figure 4. Model misfits as a function of lower-crustal (η_{LC}) and upper-mantle (η_{UM}) viscosity. (A) Contour of the first term of Equation 3, which depends on the ratio between geodetic and geologic scalar moment rate. Lower values indicate a better match between geologic and geodetic data. (B) Contour of the second term in Equation 3, which describes the misfit between the predicted vertical rate at the Central Nevada seismic belt and that measured by InSAR. (C) Contour of the third term in Equation 3, which is sensitive to the presence of undesirable time-invariant contractions in the areas surround the Central Nevada seismic belt. (D) The total constraint from all three data types combined using the method discussed in the text. Each panel has a star showing the preferred model ($\eta_{LC} = 10^{20.5}$, $\eta_{UM} = 10^{19}$ Pa-s).

the UQFD is not everywhere complete, we have speculated that there is a background disagreement rate between geodetic and geologic moment rates of a factor of 3 ± 1 , which is near the lowest value for modified R (Fig. 5B). This assertion assumes, however, that the database is equally incomplete at all locations in the Basin and Range, and hence that the anomalously high ratio in the Central Nevada seismic belt is not the result of systematically less complete geologic record. In fact, it is more likely that the opposite is true, since the Central Nevada seismic belt has been the focus of numerous studies owing to its vigorous historic seismicity and proximity to the Reno/Carson metropolitan area. In Figure 5B, lower values for modified R occur in a part of

the model space that has intermediate values for lower-crust viscosity η_{LC} ($10^{18.5}$ – $10^{20.5}$ Pa-s) and intermediate to high values for upper-mantle viscosity η_{UM} ($>10^{18.5}$ Pa-s), with the highest values for η_{UM} if η_{LC} is in a narrower band ($10^{18.5}$ – $10^{19.5}$ Pa-s). The lowest values for modified R are near the speculated background level, and hence models inside the light central region of Figure 5B are more likely to be correct models according to the first objective criteria. The similarity between Figures 5A and 5B suggests that the misfit between geodetic and geologic moment rates is controlled by the dilatational component of the geodetic strain rate field in the vicinity of the Central Nevada seismic belt. This is consistent with the observation of anomalously high geodetic

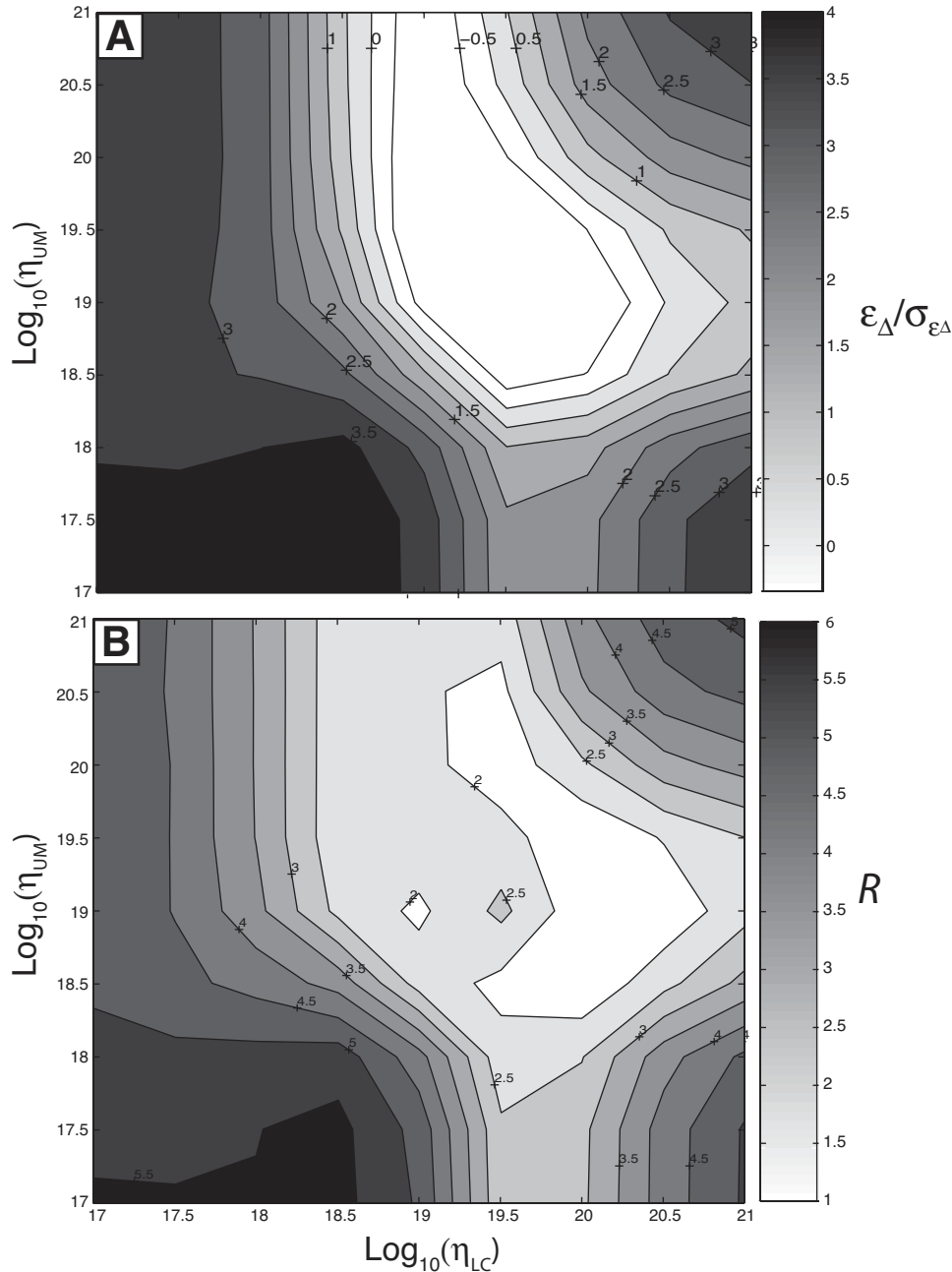


Figure 5. (A) Contour of the dilatational strain rate after correction for postseismic relaxation at the Central Nevada seismic belt normalized by its uncertainty as a function of lower-crustal (η_{LC}) and upper-mantle (η_{UM}) viscosity. Values greater than 2 indicate dilatation that is significantly larger than zero to 95% confidence. (B) Contour plot of R , the ratio of the scalar geodetic moment rate after correction for postseismic relaxation to the scalar geologic moment rate in the Central Nevada seismic belt.

dilatation at the Central Nevada seismic belt (Savage et al., 1995; Svare et al., 2002b; Hammond and Thatcher, 2004) and the likely presence of dilatation in the postseismic deformation that follows earthquakes with a normal component of slip (i.e., Pleasant Valley and Dixie Valley).

The second objective criterion eliminates viscosity models based on misfit between the vertical motion observed with InSAR and that predicted by the relaxation calculations. The maximum vertical velocity inside the Central Nevada seismic belt domain as a function of the viscosity model is shown in Figure 6. It is immediately clear that the only models that can

produce a >2 mm/yr uplift are those with a relatively high lower-crustal viscosity ($\eta_{LC} > 10^{20}$ Pa·s) and an intermediate upper-mantle viscosity (η_{UM} between $10^{18.5}$ and 10^{19} Pa·s). The range of viscosities eliminated by this criterion is very large, and is complementary to that of models eliminated by the geologic/geodetic misfit, i.e., the overlap between regions of acceptable fit in Figure 5 and Figure 6 is small. What constitutes an acceptable fit will be discussed later.

The Basin and Range is characterized by (oblique) normal faulting, so the third objective criterion is designed to eliminate models that predict time-invariant contractions, in violation of

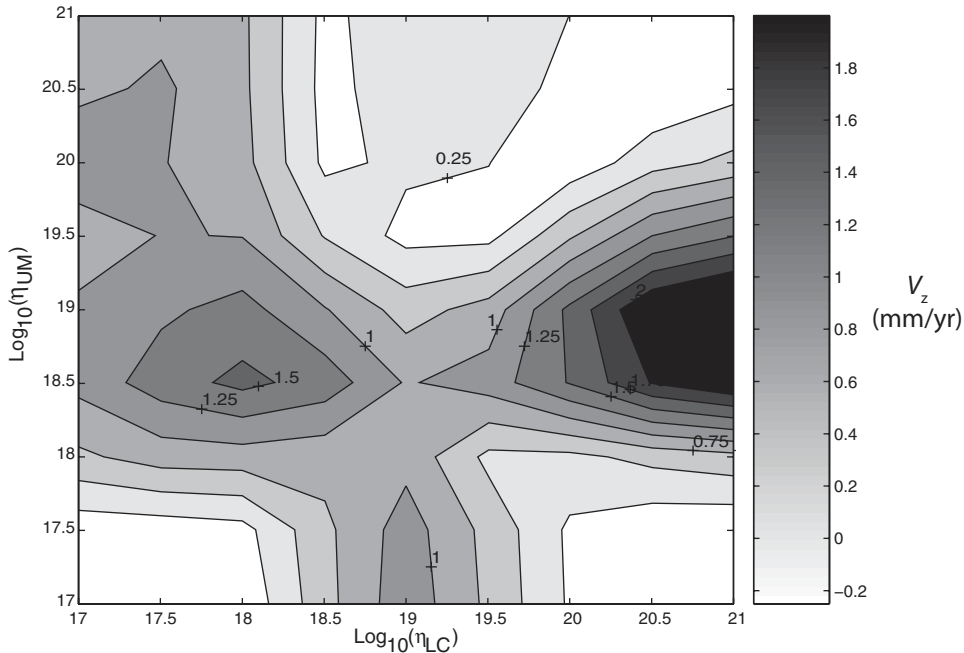


Figure 6. Contour of uplift rate (V_z) at the Central Nevada seismic belt predicted from the relaxation model as a function of lower-crustal (η_{LC}) and upper-mantle (η_{UM}) viscosity.

geological observation. The minimum and maximum time-invariant dilatational strain rates, ϵ_{Δ} , as a function of the viscosity model for each domain are shown in Table 3. None of the ϵ_{Δ} values has a normalized value below -2 , which would indicate a contraction rate that has exceeded the 2σ uncertainty level. Only the Oregon domain exhibits a normalized contraction below -1 , which indicates there may be some contraction of the entire domain. This is consistent with the presence of interseismic strain accumulation of the kind expected in the Cascadia backarc (McCaffrey et al., 2000; Miller et al., 2001b; Svarc et al., 2002a) and also with a north-south contraction of $2\text{--}3$ mm/yr observed near the Oregon-California border (Hammond and Thatcher, 2004). The minimum and maximum ϵ_{Δ} values in Table 3 also provide an illustration of the sensitivity of strain rate field to the viscoelastic properties of the lower crust and upper mantle. The range between the maximum and minimum ϵ_{Δ} is greatest for the Central Nevada seismic belt domain, consistent with its location near the historic earthquakes. The northern Walker Lane domain sees a transition from marginally insignificant to marginally significant dilatation. This implies that geodetic results that show no dilatation (e.g., Hammond and Thatcher, 2007) may have been influenced by the presence of relaxation, which can mask a small amount of secular extension. This is discussed more completely later.

Table 4 shows that correcting the geodetic strain rate field with this model makes the deformation more similar to the geologic strain rate field with respect to geographic distribution of strain rate style, if not with respect to the total magnitude of strain (which is a factor of $2\text{--}5$ smaller for the geologic model). The table shows a comparison between the strain rates inside the separate regions calculated from the geodetic strain rate model velocities, geologic data via the UQFD and Equation 1, and from

the postseismic model. This table shows the similarity between the geologic and geodetic data sets with respect to the dominance of shear strain in western Basin and Range Province, particularly the southern Walker Lane, northern Walker Lane, and Yucca Mountain regions. The only region that shows significant geodetic dilatation is the Central Nevada seismic belt, in contrast to the geologic model, which shows generally less dilatation than shear everywhere. A property of the postseismic relaxation model is that all the dilatation and most of the shear is focused at the Central Nevada seismic belt, consistent with it being the locus of the historic earthquakes used in its construction. Thus, the geodetic strains minus the postseismic relaxation model will have much less dilatation, similar to the geologic model. Note that the geodetic minus the correction will not match the geologic model exactly, because of the provincewide lower magnitude of deformation rate seen in the geologic data. However, the corrected geodetic strains provide a model that is similar to the geologic model in the sense that most dilatation has been removed, and shear strain rates at the Central Nevada seismic belt are lower than in the Walker Lane belt. The very strong correlation between R and the dilatational component of the relaxation model suggests that the model has been appropriately built to compensate for the anomalous dilatation at the Central Nevada seismic belt.

DISCUSSION

Implications for Time-Invariant Deformation of the Northern Walker Lane

The postseismic strain rates predicted by our preferred viscosity model are from the postseismic velocity field obtained

TABLE 3. DILATATIONAL STRAIN RATE (ϵ_{Δ}) FOR GEODETIC VELOCITIES CORRECTED FOR POSTSEISMIC RELAXATION

| Domain | Strain rates | | | | Normalized | | | |
|-------------------------|----------------|-----------|------|------|------------|-----------|------|------|
| | Observed | Corrected | | | Observed | Corrected | | |
| | | Min. | Max. | Best | | Min. | Max. | Best |
| Eastern Basin and Range | 1.3 ± 1.3 | 0.8 | 1.8 | 1.3 | 1.0 | 0.6 | 1.4 | 1.0 |
| CNSB | 10.5 ± 2.8 | -5.7 | 11.0 | 3.1 | 3.8 | -2.0 | 3.9 | 1.1 |
| Northern Walker Lane | 7.2 ± 3.9 | 6.5 | 10.3 | 8.8 | 1.8 | 1.7 | 2.6 | 2.3 |
| South Walker Lane | 3.9 ± 2.9 | 3.5 | 7.1 | 6.3 | 1.3 | 1.2 | 2.4 | 2.2 |
| Oregon | -3.1 ± 3.4 | -3.7 | -1.7 | -2.5 | -0.9 | -1.1 | -0.5 | -0.7 |
| Yucca Mountain | 8.0 ± 11.3 | 5.3 | 13.3 | 13.3 | 0.6 | 0.5 | 1.2 | 1.2 |

Note: The uncorrected, minimum, maximum, and preferred dilatational strain rates ϵ_{Δ} and their 1σ formal uncertainties are given in units of nanostrains (10^{-9}) per year. Normalized strain rates are the strain rates divided by their formal uncertainties. Values that are greater than 2 or less than -2 indicate 95% significant area growth rate or contractions, respectively. The difference between the maximum and minimum is a measure of the sensitivity of ϵ_{Δ} to the viscosity of the lower crust and upper mantle. The “Best” column shows the estimated secular dilatation (corrected for postseismic relaxation) inside each domain given the model with $\eta_{LC} = 10^{20.5}$ Pa-s and $\eta_{UM} = 10^{19}$ Pa-s. CNSB—Central Nevada seismic belt.

TABLE 4. GEOLOGIC, GEODETIC, AND RELAXATION MODEL STRAIN RATES INSIDE REGIONS

| Region | Geodetic | | | | Postseismic | | Geologic | | R |
|----------------------|---------------------|------------------------|-----------------|------------------------|---------------------|-----------------|---------------------|-----------------|-----|
| | ϵ_{Δ} | $\pm\sigma_{\epsilon}$ | ϵ_{xy} | $\pm\sigma_{\epsilon}$ | ϵ_{Δ} | ϵ_{xy} | ϵ_{Δ} | ϵ_{xy} | |
| East Basin and Range | 1.4 | 1.3 | 8.9 | 1.3 | 0.1 | 0.2 | 0.9 | 1.2 | 2.9 |
| Walker Lane North | 7.3 | 3.9 | 33.5 | 3.9 | -0.7 | 1.1 | 2.3 | 7.3 | 4.9 |
| Walker Lane South | 3.9 | 2.9 | 79.0 | 2.9 | -1.5 | 9.2 | 0.1 | 15.9 | 3.9 |
| Oregon | -3.0 | 3.4 | 1.0 | 3.4 | -0.1 | 0.8 | 1.3 | 0.9 | 3.9 |
| Yucca Mountain | 8.1 | 11.3 | 37.2 | 11.3 | -4.1 | 1.8 | -1.4 | 10.8 | 2.0 |
| CNSB (within 180 km) | 10.5 | 2.8 | 23.5 | 2.8 | 10.3 | 14.7 | 2.3 | 2.7 | 5.1 |
| CNSB (within 70 km) | 31.0 | 10.3 | 48.4 | 10.3 | 23.9 | 34.0 | 1.7 | 2.3 | 9.5 |

Note: Velocities used to calculate geodetic strain rates and uncertainties have not been corrected for postseismic relaxation and are from the strain rate model of Kreemer et al. (this volume). Geologic strain rates are from the UQFD (U.S. Geological Survey Quaternary Fault and Fold database), obtained in Equation 1 and shown in Figure 2. Postseismic strain rates come from the viscoelastic relaxation model. Strain rates are in nanostrains/yr. CNSB—Central Nevada seismic belt.

from the relaxation calculations. The velocities predicted from our preferred model (Fig. 7; Table DR1¹) are consistent with northwest-southeast uniaxial extension across Pleasant Valley, and significant vertical uplift of ~ 2 mm/yr predicted north of the Fairview Peak rupture. To the south, progressively greater amounts of shear deformation appear where the style of the earthquakes becomes more strike-slip. The dilatational component of postseismic transient strain rate (Fig. 8A) shows enhanced extension in the vicinity of the Central Nevada seismic belt. This patch of dilatation is spatially coincident with the anomalously high Central Nevada seismic belt dilatation rates shown in the strain rate map in a companion article to this paper (Kreemer et al., this volume). This dilatation comes mostly in the form of uniaxial northwest-southeast-directed extension, and it is visible in the detail that includes the strain rate tensor axes (Fig. 8B). The relaxation model also contains lobes of low-intensity (1–4 nanostrain/yr) contraction to the northwest and east of the Cen-

tral Nevada seismic belt historic ruptures. The lobe to the east is consistent with GPS observations of geographically broad contraction east of the Central Nevada seismic belt (Hammond and Thatcher, 2004), but it does not explain a narrow zone of contraction inferred from the single continuous GPS site LEWI on Mt. Lewis, Nevada, near Crescent Valley (Wernicke et al., 2000; Bennett et al., 2003; Friedrich et al., 2004). The significant east-west asymmetry in these contractional lobes comes from summing earthquakes with different strikes, event times, and different ruptures styles. Shorter-wavelength variations are mainly the result of geographic irregularity in the GPS sites, which causes irregular sampling of the model relaxation velocity field that is used in the strain modeling. For example, near the Owens Valley rupture at the southern end of our model, small blotches of dilatation of alternating sign exist, but these contribute negligibly to the integrated dilatation over larger regions. The transition of tensor deformation style from south to north (Fig. 8B) can also be seen in the model velocities (Fig. 7). Where the earthquake styles to the south have a larger component of right-lateral slip, we see postseismic deformation that has close to equal parts of contraction and extension, indicating shear deformation. To the

¹GSA Data Repository Item 2009001, Table DR1. Velocities from compilation of GPS, relaxation model, and secular motion, is available at www.geosociety.org/pubs/ft2009.htm, or on request from editing@geosociety.org, Documents Secretary, GSA, P.O. Box 9140, Boulder, CO 80301-9140.

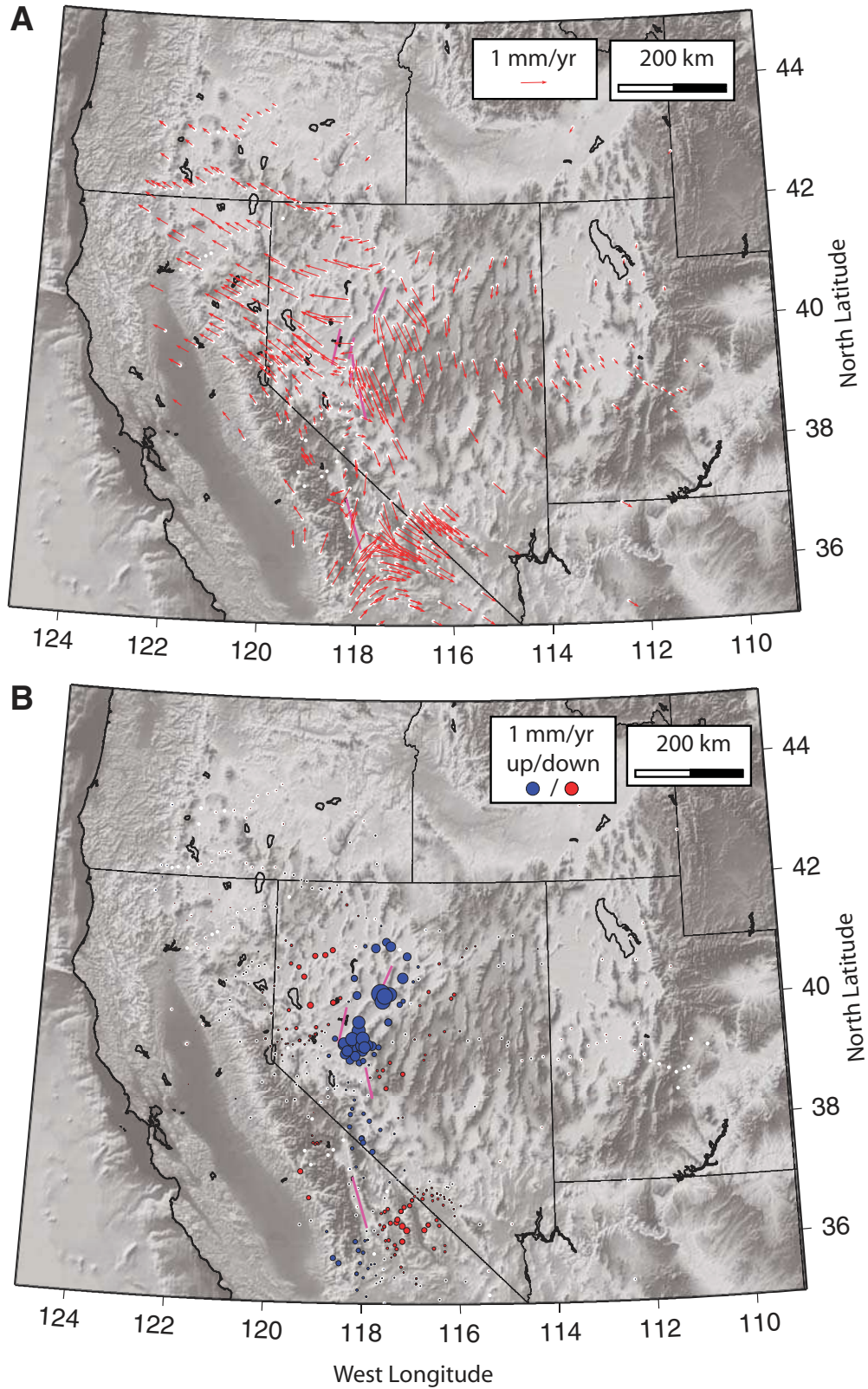


Figure 7. Postseismic relaxation velocities predicted from the preferred relaxation model ($\eta_{LC} = 10^{20.5}$, $\eta_{UM} = 10^{19}$ Pa-s), including the contributions from all the earthquakes considered in this study. (A) Red vectors show predicted horizontal velocity to the model faults (magenta line segments) at each global positioning system (GPS) site in the compilation of Kreemer et al. (this volume). (B) Vertical motion is shown blue for uplift, red for subsidence. Size of the circle indicates the vertical rate.

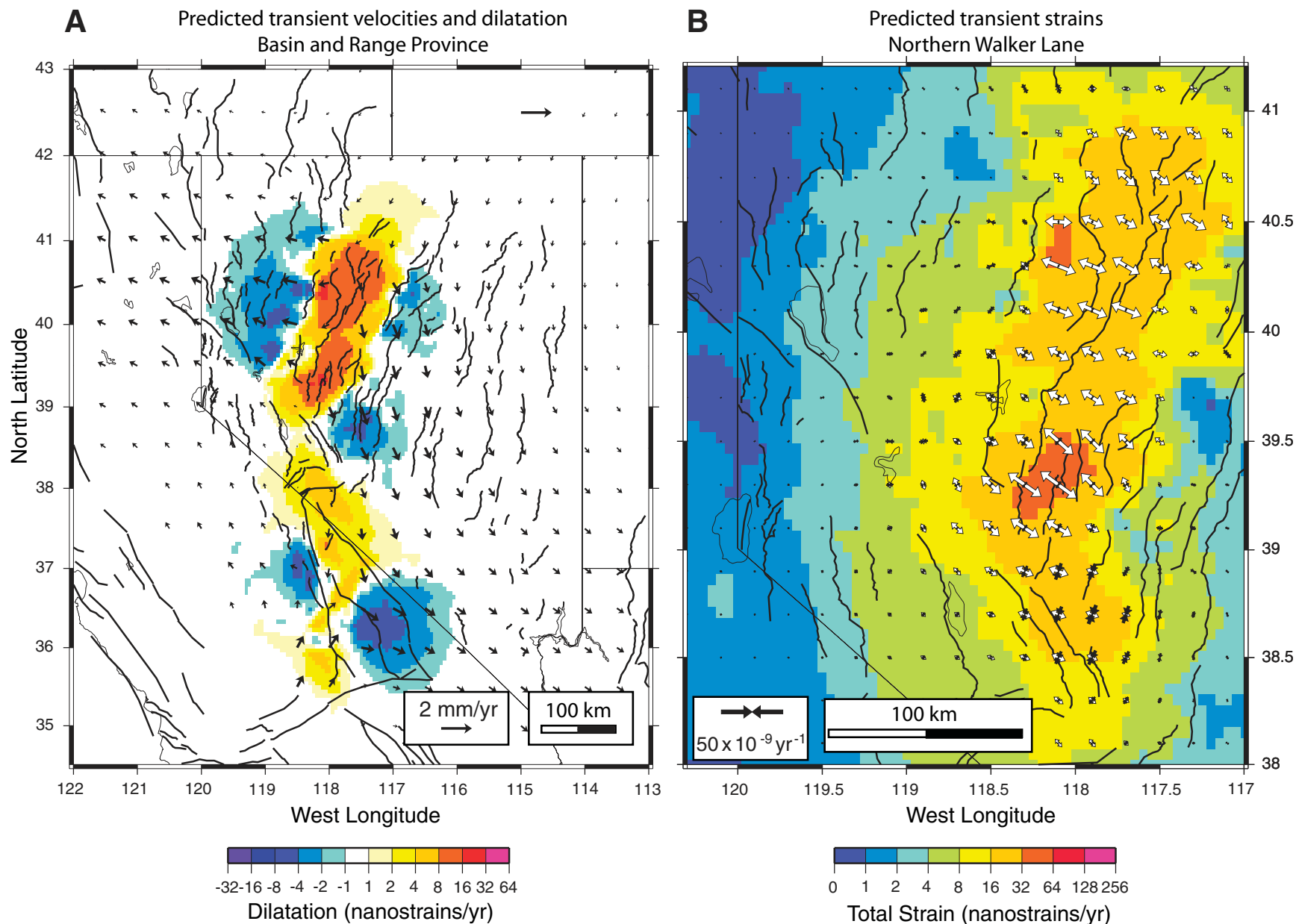


Figure 8. (A) Dilatational strain rates predicted from the preferred relaxation model velocities ($\eta_{LC} = 10^{20.5}$, $\eta_{UM} = 10^{19}$ Pa·s). This map was created using the same global positioning system (GPS) site locations as the model of Kreemer et al. (this volume), so that the effects of station distribution on the strain modeling are included. Black arrows indicate the relaxation velocities interpolated onto a regular grid. Quaternary faults are shown with black line traces. State borders and major lakes are shown with faint lines. (B) A detailed view of the northern Walker Lane. The colors now represent the amount of total strain rate, which contains both horizontal shear and dilatation. Black arrow pairs indicate tensor contraction; white arrows indicate tensor extension.

north, near the Pleasant Valley rupture, the style of extension is closer to northwest-southeast uniaxial extension, similar to the coseismic rupture there. In the vicinity of Pyramid Lake, roughly 2–4 nanostrain/yr of northwest-directed uniaxial contraction is predicted from the relaxation model.

The time-invariant deformation field is estimated by subtracting the transient velocities from the GPS velocities and then repeating the strain rate modeling of Kreemer et al. (this volume). Thus, the strain rate map of Figure 9B is expected to be in closer agreement with the deformations inferred from paleoseismological studies. A comparison of Figure 2 and Figure 9B shows that this is the case, since deformation in the time-invariant model and in the geologic model is more strongly focused into the northern Walker Lane, and there is relatively little deformation at the Central Nevada seismic belt. A single small zone of strain near longitude 118.5°W and latitude 40°N is caused by a single campaign GPS velocity (site WILD) that has a velocity that deviates by ~1 mm/yr from the smooth regional pattern. The finger of higher geologic strain rate near longitude 117°W and latitude 39°N and the Toiyabe Range (Fig. 2) is not observed in the uncorrected or corrected geodetic strain rate models (Fig. 9). It likely shows higher moment rate because of the close proximity of the Toiyabe Range fault (0.22 mm/yr), the Ione Valley fault (0.1 mm/yr), the Southwest Reese River Valley fault (0.1 mm/yr), and the Mahogany Mountain section of the Western Toiyabe Range fault zone (0.2 mm/yr).

After correction for postseismic effects, some deformation at the Central Nevada seismic belt remains, with rates that are still higher with respect to the eastern Basin and Range (Fig. 9B). In the vicinity of the Stillwater, Dixie Valley, and Fairview Peak faults, the total strain rates are 8–32 nanostrain/yr, and a bit lower near Pleasant Valley. Near the Cedar Mountain rupture, strain rates are higher, 16–32 nanostrain/yr, reduced from the 32–64 nanostrain/yr estimated before the correction. The velocity gradient across the Central Nevada seismic belt (between sites B220 and B290, Fig. 1) is 3.1 mm/yr in the GPS velocity compilation, but it has been reduced to 0.9 mm/yr in the time-invariant model. Thus, a significant fraction of the deformation at the Central Nevada seismic belt has been explained with postseismic relaxation, yet some remains and is consistent with the paleoseismological result of ~1 mm/yr extension across the Central Nevada seismic belt faults (Bell et al., 2004). The amount of velocity gradient that still exists across the Central Nevada seismic belt after the correction indicates that the belt may still have a higher rate of deformation than in the Central Basin and Range, where strain rates are close to zero (Bennett et al., 2003; Kreemer et al., this volume). The corrected rates are, however, less than what is observed in the Walker Lane to the west. Thus, these results are consistent with a greater frequency of paleoearthquakes at the Central Nevada seismic belt compared to the central Basin and Range, and the view that the Central Nevada seismic belt is a zone of deformation that extends to the northeast, possibly transferring Walker Lane dextral slip onto NNE-striking normal faults (Savage et al., 1995; Wesnousky et al., 2005; Faulds et al., 2005). For GPS sites further north and farther apart that span Pleasant

Valley, the difference owing to the correction is not as large. The relative velocity of GARL and D100 changes from 2.3 mm/yr to 1.3 mm/yr upon adjustment for postseismic deformation. In general, the magnitude of the correction decreases with distance from the Central Nevada seismic belt.

The time-invariant dilatation rate in the northern Walker Lane domain is 8.8 ± 3.9 nanostrains/yr (Table 3), just barely significant to 95% confidence, while its shear strain rate is 33.8 ± 3.9 nanostrains/yr (shear is defined as $\epsilon_1 - \epsilon_2$, where ϵ_1 and ϵ_2 are the maximum and minimum principal strain rates, respectively). This suggests that, as a whole, the northern Walker Lane acts as a right-lateral shear zone with a small component of extension. However, this extension becomes statistically significant only after the correction for postseismic relaxation from the Central Nevada seismic belt historic earthquakes has been made. Thus, in several respects, the northern Walker Lane behaves similarly to the central Walker Lane, where dextral shear rates are greater than extension rates, and the highest deformation rates are seen near the western boundary of the Walker Lane belt adjacent to the Sierra Nevada (Oldow et al., 2001; Oldow, 2003). Furthermore, these observations are consistent with campaign GPS data spanning Walker Lane between 37°N and 40°N, which show significant extension approximately normal to the trend of the shear zone but a different orientation from east to west (Oldow, 2003; Hammond and Thatcher, 2004). It is also consistent with the results of a profile of campaign GPS velocities across the northern Walker Lane in the vicinity of Pyramid Lake (Hammond and Thatcher, 2007) that did not correct for postseismic relaxation, and that observed no significant dilatation.

Implications for Basin and Range Lithospheric Rheology

The conclusions reached here are broadly consistent with Basin and Range lower-crustal and upper-mantle viscosity estimates from a number of other studies. We have summarized the values obtained by a sample of other studies in Table 2. The most common conclusion reached for the Basin and Range is that the lower crust has greater strength (i.e., higher viscosity) than the uppermost mantle on which it lies. This conclusion is consistent across studies that sample a great variety of temporal scales, from times immediately following (<3 yr) an earthquake (Pollitz et al., 2000, 2001; Pollitz, 2003) to over 10,000 yr of relaxation following the unloading owing to the draining of late Pleistocene postglacial lakes (e.g., Nakiboglu and Lambeck, 1983; Bills and May, 1987; Bills et al., 1994; Kaufmann and Amelung, 2000).

In their study of Central Nevada seismic belt rheological layering, Hetland and Hager (2003) relied on the criterion that time-invariant contraction should be explained by postseismic relaxation. Our modeling differs from theirs because we choose to exclude models that predict time-invariant contractions in any of the domains near the Central Nevada seismic belt. We do not explain the contraction east of the Central Nevada seismic belt directly, because we do not observe the contraction in our Central Basin and Range domain. This is likely owing to the fact that our domain is so large and also includes the Wasatch fault zone to the

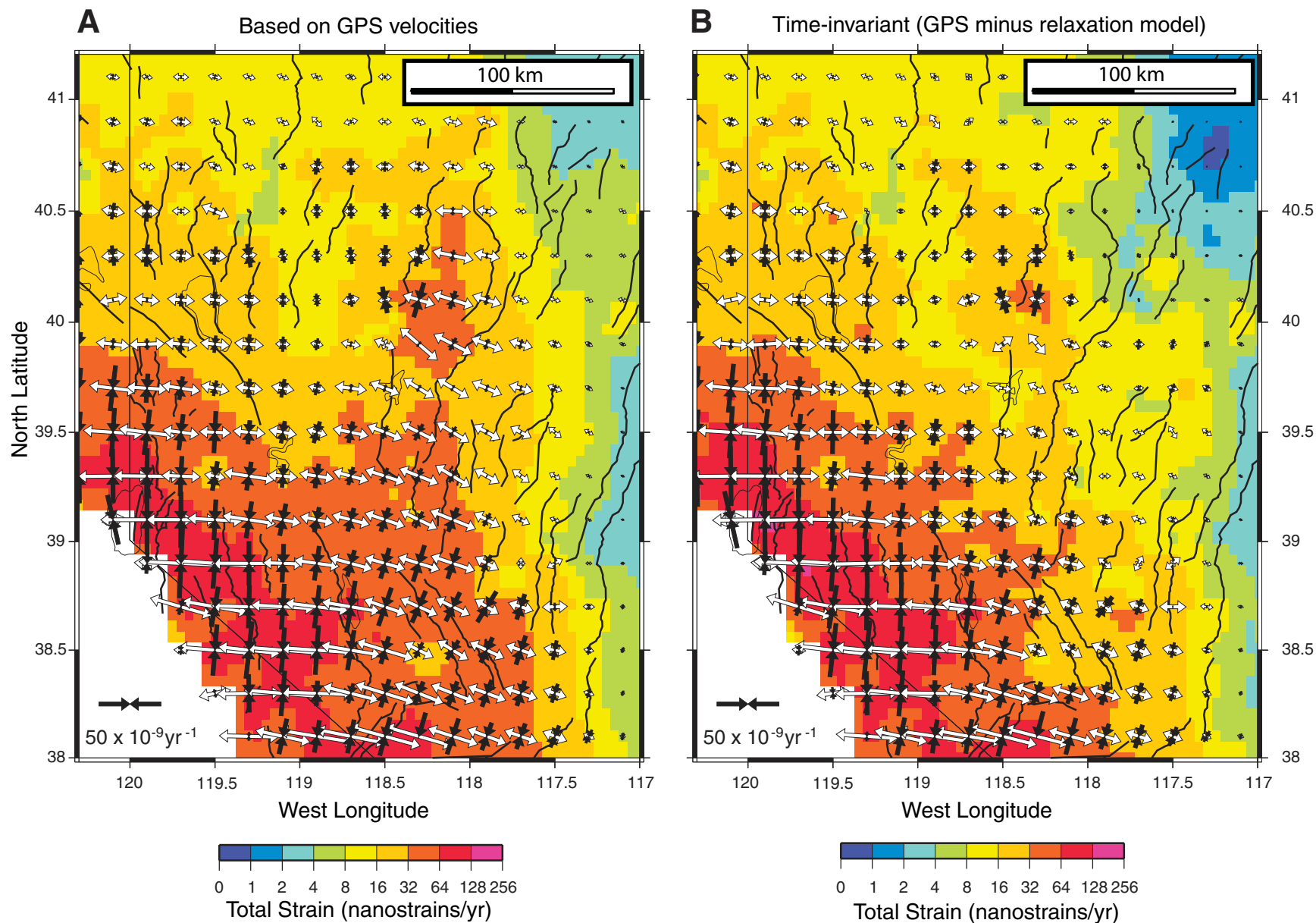


Figure 9. (A) Continuum strain rate model based on the global positioning system (GPS) velocity data. This is a detail of the map presented in Kreemer et al. (this volume). Other features are the same as B. (B) Same model except based on the time-invariant GPS velocity field obtained by subtracting the preferred relaxation model velocities ($\eta_{\text{LC}} = 10^{20.5}$, $\eta_{\text{UM}} = 10^{19}$ Pa·s) from the GPS velocities. The zone of deformation has become significantly more focused to the western edge of the Walker Lane belt.

east. However, when we use just the criterion that Central Basin and Range domain extension should be positive, amounting to approximately the same model discrimination criterion that they use, we would have estimated values of $\eta_{LC} \approx 10^{19}$ and $\eta_{UM} \geq \eta_{LC}$, which are very similar to their results. Their reliance on this criterion may explain why their result is the only one of the survey of previous results (Table 2) that indicates a lower crust that is weaker than the upper mantle.

Our results, and most of the results listed in Table 2, appear to be in disagreement with the results of others that suggest that the lower crust behaves as a low-viscosity channel through which material flows. Sometimes called the “jelly sandwich” model (Jackson, 2002), this idea has been used to explain the scarcity of earthquakes in the lower crust, the existence of metamorphic core complexes (e.g., Block and Royden, 1990), and the flatness of Moho topography despite geologic extension that is, at the surface, localized to dipping normal faults and heterogeneous over scales of hundreds of kilometers (Gans, 1987). The geodetic networks considered in this study are geographically focused in the western Great Basin, where strain rates are one to two orders of magnitude higher and metamorphic core complexes are absent. Thus, variations in crust and mantle properties may partially account for the discrepancy. However, results from several studies in the eastern Great Basin (i.e., in the vicinity of Lakes Bonneville, Mead, and Hebgen) show no strong difference in η_{LC} compared to the western Great Basin (e.g., Central Nevada seismic belt, Walker Lane, or Mohave Desert) (Table 2). According to the two-layer theory of McKenzie et al. (2000), short-wavelength Moho relief is flattened on a time scale that is proportional to the sum of crust and upper-mantle viscosities. Thus, it is possible to flatten Moho topography if the crust is stronger than the mantle, as long as the crust is weak enough to allow flow on the time scale of Basin and Range extension. For example, in the two-layer viscous model with an upper layer $10^{20.5}$ Pa·s over a half-space of 10^{19} Pa·s (values of η_{LC} and η_{UM} in our preferred model), 10 km wavelength Moho topography will relax with a characteristic decay time of 2.6 m.y. This is short enough to flatten Moho topography over the history of Basin and Range extension, and thus a weak lower crust (compared to the mantle) is not an absolute requirement to flatten Moho topography. So our model is not in conflict with the observation of a flat Moho.

An additional possibility is that lateral contrasts of lithospheric viscosity exist that can affect our results and comparisons between the Central Nevada seismic belt and other parts of the Basin and Range. Modeling of the stresses driving deformation of the western United States in the context of a thin viscous sheet suggests that the focused deformation in the westernmost part of the province is attributable to lithosphere that has a lower viscosity compared to the adjacent areas (Flesch et al., 2000). East-west asymmetry in lithospheric effective viscosity is consistent with the presence of higher heat flow (Lachenbruch and Sass, 1978; Blackwell and Steele, 1992) and lower flexural rigidity to the west (Lowry and Smith, 1995). In this study, we assumed a laterally constant viscosity, and thus our modeling does not include the

effects of east-west asymmetry in the relaxation velocity field that would be expected from an increase in viscosity east of the Central Nevada seismic belt. This can affect the strain rates that are expected from the relaxation model far from the Central Nevada seismic belt. For example, our preferred model predicts some deformation in the southern Sierra Nevada microplate (Fig. 8A), which to date has not been definitively observed. Future modeling studies will have to be undertaken to understand the effect of postseismic relaxation in the presence of lateral variations in the strength of the Basin and Range lithosphere.

Transient or power-law rheology in the upper mantle may explain relaxations that occur more quickly immediately following a large earthquake than would be expected from the longer-term (>1 yr) response assuming a Newtonian Maxwell viscoelastic model (Pollitz, 2003; Freed and Bürgmann, 2004). Our study assumes a linear response, and hence the velocity fields from the individual earthquakes can be modeled separately and then summed to represent the velocity field in the year 2005. A rheology other than Newtonian violates this assumption. If, however, the mantle were characterized with a power-law rheology that increased the inferred viscosity over time, as has been observed in the Mojave (Pollitz et al., 2001; Pollitz, 2003), then our results would tend to overestimate mantle viscosity, and our conclusions about the relative strength between the crust and upper mantle would still hold. Similarly, if the viscosity is temperature dependent, and hence smoothly decreases with depth, our modeling would be most sensitive to the upper portion of each depth interval. This would result in a systematic overestimation of the viscosity in each layer, but it would not alter the relative strength of the lower crust and upper mantle.

SUMMARY AND CONCLUSIONS

We combine horizontal GPS velocities, InSAR, and paleoseismic data with modeling of the viscoelastic postseismic response of the Central Nevada seismic belt historic earthquakes to estimate the most likely viscoelastic structure of the western Basin and Range lower crust and upper mantle. From these, we develop a correction for postseismic effects that can be used to estimate secular crustal deformation from geodetic velocities near the Central Nevada seismic belt. Our preferred model has values of $\eta_{LC} = 10^{20.5}$ Pa·s and $\eta_{UM} = 10^{19}$ Pa·s. To obtain this result, we assume that the GPS velocity field is the sum of time-invariant and transient processes, and seek models that (1) explain the mismatch between geodetic and geologically inferred slip rates, (2) explain the vertical uplift that has been observed with InSAR and (3) do not imply time-invariant contractions anywhere in the Basin and Range. This model is consistent with other geodetic studies of earthquakes and lake loading of the lithosphere, and with the observation of flat Moho topography throughout much of the Basin and Range.

We evaluate the ability that different types of data have to constrain the viscoelastic structure. We find that InSAR, GPS, and geologic data exclude different parts of the model space and

thus form complementary constraints on the viscoelastic structure. This suggests that studies that aim to constrain rheology of the lithosphere are best served by using techniques that measure both vertical and horizontal movements and that include geologic constraints on steady permanent tectonic deformation averaged over many seismic cycles.

The preferred viscosity model implies that the majority of the deformation observed at the Central Nevada seismic belt is attributable to postseismic relaxation, and that the time-invariant deformation is more tightly focused into northern Walker Lane than is inferred from the uncorrected GPS velocities. Whereas no significant dilatation was detectable before correcting for post-seismic effects, following the correction, the dilatation is significant (8.4 ± 3.9 nanostrains/yr). Thus, the Central Nevada seismic belt postseismic relaxation masks time-invariant extension in the adjacent province to the west.

The preferred model decreases the apparent discrepancy between geologically and geodetically estimates slip rates on faults at the Central Nevada seismic belt. After using this model to correct the geodetic velocity field for transient postseismic effects from historic earthquakes, the amount of geodetically inferred steady permanent extension that has occurred at the Central Nevada seismic belt is reduced, making it less anomalous with respect to the Central Basin and Range, in agreement with paleoseismic data. However, after the correction, rates of deformation at the Central Nevada seismic belt are still greater than rates in the central Basin and Range to the east, and not as great as rates in the Walker Lane belt to the west.

ACKNOWLEDGMENTS

This work was supported by the Department of Energy Geothermal Program through grant DE-FG36-02ID14311 to the Great Basin Center for Geothermal Energy and Department of Energy Yucca Mountain Project/Nevada System of Higher Education Cooperative Agreement DE-FC28-04RW12232. Special thanks are due to Fred Pollitz for sharing his VISCO1D software and assisting us with installation. We are grateful to all who contribute to and maintain the U.S. Geological Survey Quaternary Fault and Fold paleoseismic database. This manuscript was improved by careful reviews from Dennis Harry and Craig Jones.

REFERENCES CITED

Adams, K.D., Wesnousky, S.G., and Bills, B.G., 1999, Isostatic rebound, active faulting, and potential geomorphic effects in the Lake Lahontan Basin, Nevada and California: *Geological Society of America Bulletin*, v. 111, p. 1739–1756, doi: 10.1130/0016-7606(1999)111<1739:IRAFAP>2.3.CO;2.

Allmendinger, R.W., Hauge, T.A., Hauser, E.C., Potter, C.J., Klemperer, S.L., Nelson, K.D., Knuepfer, P., and Oliver, J., 1987, Overview of the COCORP 40°N transect, western United States: The fabric of an orogenic belt: *Geological Society of America Bulletin*, v. 98, p. 308–319, doi: 10.1130/0016-7606(1987)98<308:OOTCNT>2.0.CO;2.

Beanland, S., and Clark, M.M., 1994, The Owens Valley fault zone, eastern California, and surface rupture associated with the 1872 earthquake: *U.S. Geological Survey Bulletin* 1982, p. 1–29.

Bell, J.W., dePolo, C.M., Ramelli, A.R., Sarna-Wojcicki, A.M., and Meyer, C.E., 1999, Surface faulting and paleoseismic history of the 1932 Cedar Mountain earthquake area, west-central Nevada, and implications for modern tectonics of the Walker Lane: *Geological Society of America Bulletin*, v. 111, p. 791–807, doi: 10.1130/0016-7606(1999)111<0791:SFAPHO>2.3.CO;2.

Bell, J.W., Caskey, S.J., Ramelli, A.R., and Guerrieri, L., 2004, Pattern and rates of faulting in the central Nevada seismic belt, and paleoseismic evidence for prior belt-like behavior: *Bulletin of the Seismological Society of America*, v. 94, p. 1229–1254, doi: 10.1785/012003226.

Bennett, R.A., Wernicke, B.P., and Davis, J.L., 1998, Continuous GPS measurements of contemporary deformation across the northern Basin and Range Province: *Geophysical Research Letters*, v. 25, p. 563–566, doi: 10.1029/98GL00128.

Bennett, R.A., Wernicke, B.P., Niemi, N.A., Friedrich, A.M., and Davis, J.L., 2003, Contemporary strain rates in the northern Basin and Range Province from GPS data: *Tectonics*, v. 22, no. 2, 1008, doi: 10.1029/2001TC001355.

Benz, H.M., Smith, R.B., and Mooney, W.D., 1990, Crustal structure of the northwestern Basin and Range Province from the 1986 Program for Array Seismic Studies of the Continental Lithosphere seismic experiment: *Journal of Geophysical Research*, v. 95, p. 21,823–21,842, doi: 10.1029/JB095iB13p21823.

Bills, B.G., and May, G.M., 1987, Lake Bonneville: Constraints on lithospheric thickness and upper mantle viscosity from isostatic warping of Bonneville, Provo and Gilbert stage shorelines: *Journal of Geophysical Research*, v. 92, p. 11,493–11,508, doi: 10.1029/JB092iB11p11493.

Bills, B.G., Currey, D.R., and Marshall, G.A., 1994, Viscosity estimates for the crust and upper-mantle from patterns of shoreline deformation in the Eastern Great Basin: *Journal of Geophysical Research*, v. 99, p. 22,059–22,086, doi: 10.1029/94JB01192.

Bills, B.G., Adams, K.D., and Wesnousky, S.G., 2007, Viscosity structure of the crust and upper mantle in western Nevada from isostatic rebound patterns of Lake Lahontan shorelines: *Journal of Geophysical Research*, v. 112, B06405, doi: 10.1029/2005JB003941.

Blackwell, D.D., and Steele, J.L., 1992, *Geothermal Map of North America: Boulder, Colorado, Geological Society of America, scale 1:5000000.*

Blewitt, G., Argus, D.F., Bennett, R.A., Bock, Y., Calais, E., Craymer, M., Davis, J.L., Dixon, T.H., Freymueller, J.T., Herring, T.A., Johnson, D., Larson, K.M., Miller, M.M., Sella, G.F., Snay, R.A., and Tamissiea, M., 2005, A stable North America reference frame (SNARF): First release: UNAVCO-IRIS Joint Workshop: Stevenson, Washington.

Block, L., and Royden, L.H., 1990, Core complex geometries and regional scale flow in the lower crust: *Tectonics*, v. 9, p. 557–567, doi: 10.1029/TC009i004p00557.

Cao, T., Bryant, W.A., Rowshandel, B., Branum, D., and Wills, C.J., 2003, The Revised 2002 California Probabilistic Seismic Hazard Maps: California Geological Survey Open-File Report 96-08, 12 p.

Caskey, J.S., Wesnousky, S.G., Zhang, P., and Slemmons, B.D., 1996, Surface faulting of the 1954 Fairview Peak ($M_s=7.2$) and Dixie Valley ($M_s=6.9$) earthquakes, central Nevada: *Bulletin of the Seismological Society of America*, v. 86, p. 761–787.

Caskey, J.S., Bell, J.W., Slemmons, B.D., and Ramelli, A.R., 2000, Historical surface faulting and paleoseismology of the central Nevada seismic belt, in Lageson, D.R., Peters, S.G., and Lahren, M.M., eds., *Great Basin and Sierra Nevada: Boulder, Colorado, Geological Society of America Field Guide 2*, p. 23–44.

Caskey, J.S., Bell, J.W., Ramelli, A.R., and Wesnousky, S.G., 2004, Historic surface faulting and paleoseismicity in the area of the 1954 Rainbow Mountain–Stillwater earthquake sequence, central Nevada: *Bulletin of the Seismological Society of America*, v. 94, p. 1255–1275, doi: 10.1785/012003012.

Chang, W.-L., and Smith, R.B., 2008, Lithospheric rheology from post-seismic deformation of a $M7.5$ normal faulting earthquake with implications for continental kinematics: *Journal of Geophysical Research* (in press).

DeMets, C., and Dixon, T.H., 1999, New kinematic models for Pacific–North America motion from 3 Ma to present: I. Evidence for steady motion and biases in the NUVEL-1A model: *Geophysical Research Letters*, v. 26, p. 1921–1924, doi: 10.1029/1999GL900405.

dePolo, C.M., and Anderson, J.G., 2000, Estimating the slip rates of normal faults in the Great Basin, USA: *Basin Research*, v. 12, p. 227–240, doi: 10.1046/j.1365-2117.2000.00131.x.

Dixon, T.H., Norabuena, E., and Hotaling, L., 2003, Paleoseismology and Global Positioning System: Earthquake-cycle effects and geodetic versus geologic

- fault slip rates in the eastern California shear zone: *Geology*, v. 31, p. 55–58, doi: 10.1130/0091-7613(2003)031<0055:PAGPSE>2.0.CO;2.
- Doser, D.I., 1986, Earthquake processes in the Rainbow Mountain–Fairview Peak–Dixie Valley, Nevada, Region 1954–1959: *Journal of Geophysical Research*, v. 91, p. 12,572–12,586, doi: 10.1029/JB091iB12p12572.
- Doser, D.I., 1988, Source parameters of earthquakes in the Nevada seismic zone, 1915–1943: *Journal of Geophysical Research*, v. 93, p. 15,001–15,015, doi: 10.1029/JB093iB12p15001.
- Dziewonski, A.M., and Anderson, D.L., 1981, Preliminary reference Earth model: *Physics of the Earth and Planetary Interiors*, v. 25, p. 297–356, doi: 10.1016/0031-9201(81)90046-7.
- Faulds, J.E., Henry, C.D., and Hinz, N.H., 2005, Kinematics of the northern Walker Lane: An incipient transform fault along the Pacific–North American plate boundary: *Geology*, v. 33, p. 505–508, doi: 10.1130/G21274.1.
- Fialko, Y., 2004, Evidence of fluid-filled upper crust from observations of post-seismic deformation due to the 1992 M_w 7.3 Landers earthquake: *Journal of Geophysical Research*, v. 109, B08401, doi: 10.1029/2004JB002985.
- Flesch, L.M., Holt, W.E., Haines, A.J., and Shen-Tu, B., 2000, Dynamics of the Pacific–North America plate boundary in the western United States: *Science*, v. 287, p. 834–836, doi: 10.1126/science.287.5454.834.
- Freed, A.M., and Bürgmann, R., 2004, Evidence of power-law flow in the Mojave Desert mantle: *Nature*, v. 430, p. 548–551, doi: 10.1038/nature02784.
- Freund, L.B., and Barnett, D.M., 1976, A two-dimensional analysis of surface deformation due to dip-slip faulting: *Bulletin of the Seismological Society of America*, v. 66, p. 667–675.
- Friedrich, A.M., Wernicke, B.P., Niemi, N.A., Bennett, R.A., and Davis, G.A., 2003, Comparison of geodetic and geologic data from the Wasatch region, Utah, and implications for the spectral character of Earth deformation at periods of 10 to 10 million years: *Journal of Geophysical Research*, v. 108, no. B4, 2199, doi: 10.1029/2001JB000682.
- Friedrich, A.M., Lee, J., Wernicke, B.P., and Sieh, K., 2004, Geologic context of geodetic data across a Basin and Range normal fault, Crescent Valley, Nevada: *Tectonics*, v. 23, p. TC2015, doi: 10.1029/2003TC001528.
- Gans, P.B., 1987, An open-system, two-layer crustal stretching model for the eastern Great Basin: *Tectonics*, v. 6, p. 1–12, doi: 10.1029/TC006001p00001.
- Gilbert, H., and Sheehan, A.F., 2004, Images of crustal variations in the intermountain west: *Journal of Geophysical Research*, v. 109, B03306, doi: 10.1029/2003JB002730.
- Gourmelen, N., and Amelung, F., 2005, Post-seismic deformation in the Central Nevada seismic belt detected by InSAR: Implications for Basin and Range dynamics: *Science*, v. 310, p. 1473–1476, doi: 10.1126/science.1119798.
- Haller, K.M., Wheeler, R.L., and Rukstales, K.S., 2002, Documentation of Changes in Fault Parameters for the 2002 National Seismic Hazard Maps: Conterminous United States except California: U.S. Geological Survey Open-File Report 02-467, 34 p.
- Hammond, W.C., and Thatcher, W., 2004, Contemporary tectonic deformation of the Basin and Range Province, western United States: 10 years of observation with the global positioning system: *Journal of Geophysical Research*, v. 109, p. B08403, doi: 10.1029/2003JB002746.
- Hammond, W.C., and Thatcher, W., 2005, Northwest Basin and Range tectonic deformation observed with the global positioning system, 1999–2003: *Journal of Geophysical Research*, v. 110, p. B10405, doi: 10.1029/2005JB003678.
- Hammond, W.C., and Thatcher, W., 2007, Crustal deformation across the Sierra Nevada, northern Walker Lane, Basin and Range transition, western United States measured with GPS, 2000–2004: *Journal of Geophysical Research*, v. 112, p. B05411, doi: 10.1029/2006JB004625.
- Hearn, E.H., 2003, What can GPS data tell us about the dynamics of post-seismic deformation?: *Geophysical Journal International*, v. 155, p. 753–777, doi: 10.1111/j.1365-246X.2003.02030.x.
- Hetland, E.A., and Hager, B.H., 2003, Postseismic relaxation across the Central Nevada seismic belt: *Journal of Geophysical Research*, v. 108, 2394, doi: 10.1029/2002JB002257.
- Hodgkinson, K.M., Stein, R.S., and Marshall, G., 1996, Geometry of the 1954 Fairview Peak–Dixie Valley earthquake sequence from a joint inversion of leveling and triangulation data: *Journal of Geophysical Research*, v. 101, p. 25,437–25,457, doi: 10.1029/96JB01643.
- Holbrook, S.W., 1990, The crustal structure of the northwestern Basin and Range Province, Nevada, from wide-angle seismic data: *Journal of Geophysical Research*, v. 95, p. 21,843–21,869, doi: 10.1029/JB095iB13p21843.
- Jackson, J., 2002, Strength of the continental lithosphere; time to abandon the jelly sandwich?: *GSA Today*, v. 12, no. 9, p. 4–10, doi: 10.1130/1052-5173(2002)012<0004:SOTCLT>2.0.CO;2.
- Kaufmann, G., and Amelung, F., 2000, Reservoir-induced deformation and continental rheology in vicinity of Lake Mead, Nevada: *Journal of Geophysical Research*, v. 105, p. 16,341–16,358, doi: 10.1029/2000JB900079.
- Kostrov, V.V., 1974, Seismic moment and energy of earthquakes, and seismic flow of rocks: *Izvestiya, Physics of the Solid Earth*, v. 1, p. 23–44 (English translation).
- Kreemer, C., Haines, J.A., Holt, W.E., Blewitt, G., and Lavallee, D., 2000, On the determination of the Global Strain Rate model: *Earth Planets Space*, v. 52, p. 765–770.
- Kreemer, C., Blewitt, G., and Hammond, W.C., 2009, this volume, Geodetic constraints on contemporary deformation in the northern Walker Lane: 2. Velocity and strain rate tensor analysis, *in* Oldow, J.S., and Cashman, P.H., eds., Late Cenozoic Structure and Evolution of the Great Basin–Sierra Nevada Transition: Geological Society of America Special Paper 447, doi: 10.1130/2009.2447(02).
- Lachenbruch, A.H., and Sass, J.H., 1978, Models of extending lithosphere and heat flow in the Basin and Range Province, *in* Smith, R.B., and Eaton, G.P., eds., Cenozoic Tectonics and Regional Geophysics of the Western Cordillera: Geological Society of America Memoir 152, p. 209–250.
- Lee, J., Spencer, J., and Owen, L., 2001, Holocene slip rates along the Owens Valley fault, California: Implications for the recent evolution of the Eastern California shear zone: *Geology*, v. 29, p. 819–822, doi: 10.1130/0091-7613(2001)029<0819:HSRATO>2.0.CO;2.
- Lowry, A.R., and Smith, R.B., 1995, Strength and rheology of the western U.S. Cordillera: *Journal of Geophysical Research*, v. 100, p. 17,947–17,963, doi: 10.1029/95JB00747.
- McCaffrey, R., Long, M.D., Goldfinger, C., Zwick, P.C., Nabelek, J.L., Johnson, C.K., and Smith, C., 2000, Rotation and plate locking at the southern Cascadia subduction zone: *Geophysical Research Letters*, v. 27, p. 3117–3120, doi: 10.1029/2000GL011768.
- McKenzie, D., Nimmo, F., Jackson, J.A., Gans, P.B., and Miller, E.L., 2000, Characteristics and consequences of flow in the lower crust: *Journal of Geophysical Research*, v. 105, no. B5, p. 11,029–11,046.
- Miller, M.M., Johnson, D.J., and Dixon, T.H., 2001a, Refined kinematics of the eastern California shear zone from GPS observations, 1993–1998: *Journal of Geophysical Research*, v. 106, p. 2245–2263, doi: 10.1029/2000JB900328.
- Miller, M.M., Johnson, D.J., Rubin, C.M., Dragert, H., Wang, K., Qamar, A., and Goldfinger, C., 2001b, GPS-determination of along-strike variation in Cascadia margin kinematics: Implications for relative plate motion, subduction zone coupling, and permanent deformation: *Tectonics*, v. 20, p. 161–176, doi: 10.1029/2000TC001224.
- Murray, J.R., Segall, P., Cervelli, P., Prescott, W.H., and Svare, J.L., 2001, Inversion of GPS data for spatially variable slip-rate on the San Andreas fault near Parkfield, CA: *Geophysical Research Letters*, v. 28, p. 359–362, doi: 10.1029/2000GL011933.
- Nakiboglu, S.M., and Lambeck, K., 1983, A reevaluation of the isostatic rebound of Lake Bonneville: *Journal of Geophysical Research*, v. 88, p. 10,439–10,447, doi: 10.1029/JB088iB12p10439.
- Nishimura, T., and Thatcher, W., 2003, Rheology of the lithosphere inferred from postseismic uplift following the 1959 Hebgen Lake earthquake: *Journal of Geophysical Research*, v. 108, no. B8, 2389, doi: 10.1029/2002JB002191.
- Nur, A., and Mavko, G., 1974, Postseismic viscoelastic rebound: *Science*, v. 183, p. 204–206, doi: 10.1126/science.183.4121.204.
- Oldow, J.S., 2003, Active transtensional boundary zone between the western Great Basin and Sierra Nevada block, western U.S. Cordillera: *Geology*, v. 31, p. 1033–1036, doi: 10.1130/G19838.1.
- Oldow, J.S., Aiken, C.L.V., Hare, J.L., Ferguson, J.F., and Hardyman, R.F., 2001, Active displacement transfer and differential block motion within the central Walker Lane, western Great Basin: *Geology*, v. 29, p. 19–22, doi: 10.1130/0091-7613(2001)029<0019:ADTADB>2.0.CO;2.
- Panah, A., Anderson, J.G., and Kreemer, C., 2006, Comparison of seismic and geodetic scalar moment rates across the Basin and Range Province: *Bulletin of the Seismological Society of America*, v. 96, p. 11–32, doi: 10.1785/0120040166.
- Pollitz, F.F., 1997, Gravitational-viscoelastic postseismic relaxation on a layered spherical Earth: *Journal of Geophysical Research*, v. 102, p. 17,921–17,941, doi: 10.1029/97JB01277.
- Pollitz, F.F., 2003, Transient rheology of the uppermost mantle beneath the Mojave Desert, California: *Earth and Planetary Science Letters*, v. 215, p. 89–104, doi: 10.1016/S0012-821X(03)00432-1.
- Pollitz, F.F., Peltzer, G., and Bürgmann, R., 2000, Mobility of continental mantle: Evidence from postseismic geodetic observation following the 1992

- Landers earthquake: *Journal of Geophysical Research*, v. 105, p. 8035–8054, doi: 10.1029/1999JB900380.
- Pollitz, F.F., Wicks, C.W., and Thatcher, W., 2001, Mantle flow beneath a continental strike-slip fault: Postseismic deformation after the 1999 Hector Mine earthquake: *Science*, v. 293, p. 1814–1818, doi: 10.1126/science.1061361.
- Pollitz, F.F., Bukun, W.H., and Nyst, M., 2004, A physical model for strain accumulation in the San Francisco Bay region: Stress evolution since 1838: *Journal of Geophysical Research*, v. 109, B11408, doi: 10.1029/2004JB003003.
- Savage, J.C., and Burford, R.O., 1973, Geodetic determination of relative plate motion in central California: *Journal of Geophysical Research*, v. 78, p. 832–845, doi: 10.1029/JB078i005p00832.
- Savage, J.C., and Hastie, L.M., 1969, A dislocation model for the Fairview Peak, Nevada, earthquake: *Bulletin of the Seismological Society of America*, v. 59, p. 1937–1948.
- Savage, J.C., and Prescott, W.H., 1978, Asthenosphere readjustment and the earthquake cycle: *Journal of Geophysical Research*, v. 83, p. 3369–3376, doi: 10.1029/JB083iB07p03369.
- Savage, J.C., Lisowski, M., Svarc, J.L., and Gross, W.K., 1995, Strain accumulation across the central Nevada seismic zone, 1973–1994: *Journal of Geophysical Research*, v. 100, p. 20,257–20,269, doi: 10.1029/95JB01872.
- Savage, J.C., Gan, W., and Svarc, J.L., 2001, Strain accumulation and rotation in the Eastern California shear zone: *Journal of Geophysical Research*, v. 106, p. 21,995–22,007, doi: 10.1029/2000JB000127.
- Sawyer, T.L., Briggs, R.W., and Ramelli, A.R., 2005, Late Quaternary activity of the Southern Mohawk Valley fault zone, northeastern California: *Seismological Research Letters*, v. 76, p. 248.
- Sella, G.F., Dixon, T.H., and Mao, A., 2002, REVEL: A model for recent plate velocities from space geodesy: *Journal of Geophysical Research*, v. 107, no. B4, 2081, doi: 10.1029/2000JB000033.
- Shen-Tu, B., Holt, W.E., and Haines, J.A., 1999, Deformation kinematics in the western United States determined from Quaternary fault slip rates and recent geodetic data: *Journal of Geophysical Research*, v. 104, p. 28,927–28,955, doi: 10.1029/1999JB900293.
- Slemmons, B.D., 1957, Geological effects of the Dixie Valley–Fairview Peak, Nevada earthquakes of December 16, 1954: *Bulletin of the Seismological Society of America*, v. 47, p. 353–375.
- Snay, R.A., Cline, M.W., and Timmermann, E.L., 1985, Dislocation models for the 1954 earthquake sequence in Nevada: U.S. Geological Survey Open-File Report 89-290, p. 531–555.
- Svarc, J.L., Savage, J.C., Prescott, W.H., and Murray, M.H., 2002a, Strain accumulation and rotation in western Oregon and southwestern Washington: *Journal of Geophysical Research*, v. 107, no. B5, 2087, doi: 10.1029/2001JB000625.
- Svarc, J.L., Savage, J.C., Prescott, W.H., and Ramelli, A.R., 2002b, Strain accumulation and rotation in western Nevada, 1993–2000: *Journal of Geophysical Research*, v. 107, no. B5, 2090, doi: 10.1029/2001JB000579.
- Thatcher, W., Foulger, G.R., Julian, B.R., Svarc, J.L., Quilty, E., and Bawden, G.W., 1999, Present-day deformation across the Basin and Range Province, western United States: *Science*, v. 283, p. 1714–1718, doi: 10.1126/science.283.5408.1714.
- Wallace, R.E., 1984a, Faulting related to the 1915 earthquakes in Pleasant Valley, Nevada: U.S. Geological Survey Professional Paper 1274-A, p. A1–A33.
- Wallace, R.E., 1984b, Patterns and timing of late Quaternary faulting in the Great Basin Province and relation to some regional tectonic features: *Journal of Geophysical Research*, v. 89, p. 5763–5769, doi: 10.1029/JB089iB07p05763.
- Wernicke, B.P., Friedrich, A.M., Niemi, N.A., Bennett, R.A., and Davis, J.L., 2000, Dynamics of plate boundary fault systems from Basin and Range Geodetic Network (BARGEN) and Geologic Data: *GSA Today*, v. 10, no. 11, p. 1–7.
- Wesnousky, S.G., Baron, A.D., Briggs, R.W., Caskey, J.S., Kumar, S.J., and Owen, L., 2005, Paleoseismic transect across the northern Great Basin: *Journal of Geophysical Research*, v. 110, p. B05408, doi: 10.1029/2004JB003283.

MANUSCRIPT ACCEPTED BY THE SOCIETY 21 JULY 2008